Master's Thesis 2014

Candidate: Christian Berg

Title: Viscoelastic entrance flow of Hydrolized Polyacrylamide (HPAAM)

Telemark University College

Faculty of Technology
Kjølnes
3914 Porsgrunn
Norway
Lower Degree Programmes – M.Sc. Programmes – Ph.D. Programmes

Telemark University College
Faculty of Technology
M.Sc. Programme
MASTER'S THESIS, COURSE CODE FMH606

Student:	**Christian Berg**		
Thesis title:	**Viscoelastic entrance flow of Hydrolized Polyacrylamide (HPAAM)**		
Signature:	. . . . .		
Number of pages:	81		
Keywords:	Viscoelastic flow, Haagen Pouisulle, Oldroyd-B, HPAAM, Polyacrylamide EOR, Polymer flooding		
Supervisor:	Knut Vågsæther	sign.:	. . . . .
2nd Supervisor:	Christian Rosenkilde	sign.:	. . . . .
Censor:	Vidar Mathiesen	sign.:	. . . . .
External partner:	Statoil	sign.:	. . . . .
Availability:	Open		

Archive approval (supervisor signature)**:** sign.: . . . . . **Date :** . . . . . .

Abstract:

The use of polymers in polymer/water flooding enhanced oil recovery (EOR) is a technique used since just after World War 2, and with several full scale fields in operation. Increasing oil prices and more challenging reservoirs make polymer flooding even more interesting as a EOR method in modern times.

One of the most common EOR polymers, hydrolyzed polyacrylamide (HPAAM) is a synthetically produced water soluble high molecular weight polymer. HPAAM acts shear thinning in bulk rheological measurements, but when flooded through porous media a rapid increase in resistance to flow (increasing apparent viscosity) is observed with flow rate, starting at a critical flow rate. This effect is poorly understood, but thought to be due to viscoelasticity, and the polymer molecules uncoiling in the "stretch" flow in pore entrances. After a local maximum, the apparent viscosity decrease, thought to be due to mechanical degradation mechanisms.

The flow of HPAAM in short and long capillary tubes has been studied experimentally, and found to exhibit the same behaviour as in porous media. A local maximum in apparent viscosity (caused by an inlet effect) and degradation after this local maximum was also observed.

A Oldroyd-B viscoelastic model was implemented in ANSYS Fluent to study the inlet pressure drop observed experimentally, but although the model shows promise for predicting some viscoelastic phenomena it fails to predict the high inlet pressure losses.

CFD simulations with Newtonian fluids were used to study the proportionality between max stretch rate and wall shear rate for the experimental geometry, often considered proportional in literature. It was found that for the experimental geometry the proportionality seems Reynolds number dependent, approaching a constant value. The effect of having a highly viscoelastic fluid in the inlet, and its influence on the flow is uncertain, but literature shows that viscoelasticity can have a high impact on entrance flow.

Table of contents

Preface

This thesis presents the work of my Master Thesis work, carried out during spring 2014 at Telemark University College (TUC), Porsgrunn, with Statoil as a project partner. This thesis is carried out in partial fulfilment of my Master of Science (MSc) degree at Telemark University College during the fourth semester.

The objective of the work has been to study the "strange" and poorly understood flow behaviour of hydrolized polyacrylamide (HPAAM) in porous media. It has been challenging and rewarding starting with only a few theories and a high accuracy pump, and then developing procedures etc. trying to study the "shear thickening" behaviour of HPAAM in porous media. Work was also done on simulations using CFD, sadly not being able to capture the experimental results. Having had the chance to work with custom written CFD libraries for Fluent was still very rewarding.

I would like to thank my supervisor Knut Vågsæther, for guidance through the project and the rest of the gas explosion research group at TUC for asking questions and discussing results and theories.

I would also like to thank Statoil, and Christian Rosenkilde for initiating this project, and for discussions on results and theories underway. I would also like to thank Kjetil Brakstad and Jens Bragdø Smith at Statoil for valuable discussions on results during my work, and help with getting solutions and equipment I needed.

Last but not least I would like to thank my fiancée for support, help on corrections and for bearing with me when my mind at times have been wandering during this work.

Porsgrunn 2.6.2014

Christian Berg

1 Introduction

Enhanced oil recovery (EOR) through water injection and polymer injection is something that has been used for decades, but with increasing popularity and potential due to higher oil prices and more challenging reservoirs.

One of the most common polymer-injection polymers Hydrolized PolyAcrylAmide (HPAAM), is a water soluble polymer forming a complex fluid with water having multiple non-Newtonian effects. This make numerical predictions challenging in reservoirs and process equipment alike. HPAAM has also been shown to mechanically degrade, leading to a loss of viscosity and thus its main mechanism as a EOR method.

When HPAAM is studied in common rheometers under shear it acts shear thinning and the results fit well with traditional empirically derived non-Newtonian models. The “strange” effects happen when HPAAM is flooded through porous media, the fluid exhibiting a rapidly increasing apparent viscosity at a critical rate and thus departing completely from the shear thinning bulk rheology measurements. This effect is thought to be due to stretching deformations of the fluid in porous media at a microscopic scale, leading to uncoiling of polymer molecules, but the mechanisms is poorly understood. Traditional EOR literature often name this increase in apparent viscosity “shear thickening”, and that the fluid has a “shear thickening” in porous media not being observed in the laboratory.

The main goal of this work was to study this thickening effect observed in porous media in more easily defined geometries, and studying whether the thickening effect is due to “stretch” or just a thickening of the fluid at high shear laminar flows.

The thickening effect observed in porous media has in this work been studied experimentally by flowing HPAAM through capillary tubes at different lengths as well as through CFD simulations to understand the deformations occurring in the experimental geometry.

The thesis is divided into 5 main chapters. Chapter 2 aims to give a brief and general introduction into EOR using polymer solutions, polymer rheology and introducing some dimensionless groups before the literature review in chapter 3. Chapter 4 aims to give a general introduction into continuum physics and modelling of non-Newtonian complex fluids. In chapter 5 and 6 the work done experimentally and using CFD is described with results and discussion.

2 Background

The use of secondary recovery methods such as waterflooding or gas flooding for pressure support is a technique that has been utilized since just after world war 2. The application of water soluble polymers in "viscous waterflooding" started in the 1960's. There has been a considerable amount of research on this topic since then and several full-scale field applications [1]. This chapter aims to give a general (and simple) introduction to polymer flooding and the rheology of typical diluted polymer solutions.

2.1 Enhanced oil recovery

Oil recovery strategies have traditionally been divided into three stages, primary, secondary and tertiary recovery, usually utilized in chronological order for a reservoir. Primary recovery is recovery through natural energy providing mechanisms in the reservoir, such as gas cap drive, oil expansion, gravity drainage etc. Secondary recovery techniques are usually used when production decline using primary reservoir drives. Secondary recovery techniques are traditionally pressure support in the reservoir through injection of gas or water. Water injection is also known as waterflooding, and is the most common secondary recovery strategy. Tertiary recovery methods is the injection of miscible gasses or chemicals after declining production using secondary methods [1]. The use of polymer flooding, i.e. injecting polymer-water solutions can by the above definition be defined as a tertiary recovery method or secondary recovery method. The similarity with a secondary recovery waterflood is due to many of the mechanism involved being similar to a waterflood with the displacing polymer solution having a different rheology than water. Many reservoirs that have challenging conditions with for instance poor natural pressure support or viscous oil may benefit greatly from using enhanced oil recovery methods from the start up of production [1].

2.2 Oil-recovery polymers- Hydrolyzed Polyacrylamide (HPAAM)

The polymer studied in this work, Hydrolysed Polyacrylamide (HPAAM) is a synthetically manufactured, high molecular weight water soluble polymer with a molecular structure as seen in Figure 2-1.

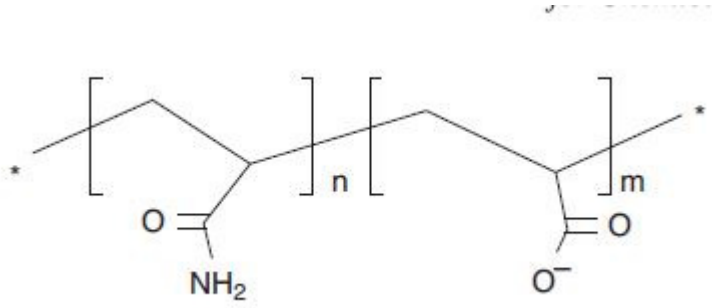

Figure 2-1 Molecular structure of hydrolyzed polyacrylamide [2].

In general HPAAM behaviour in diluted solutions have some main properties affecting solution properties other than polymer concentration, namely degree of hydrolysis, solvent ion concentration and polymer molecular weight. Figure 2-2 show the effect of polymer concentration and molecular weight on solution viscosity at a given shear rate. In general, higher molecular weight at a given concentration, or higher concentration at a given molecular weight increase the viscosity. Ions present in the solution decrease the viscosity by causing the polymers to coil up such that they have a less significant expansion in the solution[2].

Since the mean polymer molecular weight is a important factor for the solution viscosity any degradation of the polymer chains cause a decrease in viscosity. In general degradation of HPAAM solutions happen through three main routes, chemical, thermal and mechanical [2].

Chemical degradation happen from free radicals in the solution reacting with the polymer backbone, reducing molecular weight and viscosity. This is often caused by Red/Ox systems such as oxygen and impurities present in the solution, and can be observed as oxidative degradation if solutions are prepared from water that contain contaminants in combination with exposure to atmospheric oxygen[2].

Thermal degradation depends on temperature and polymer properties. For regular HPAAM polymers a increased temperature cause a increase in hydrolysis, creating more functional anionic groups [2].

Mechanical degradation occurs due to excessive deformations in the polymer solution, thought to cut the polymer chains and thus reducing the mean molecular weight[3].

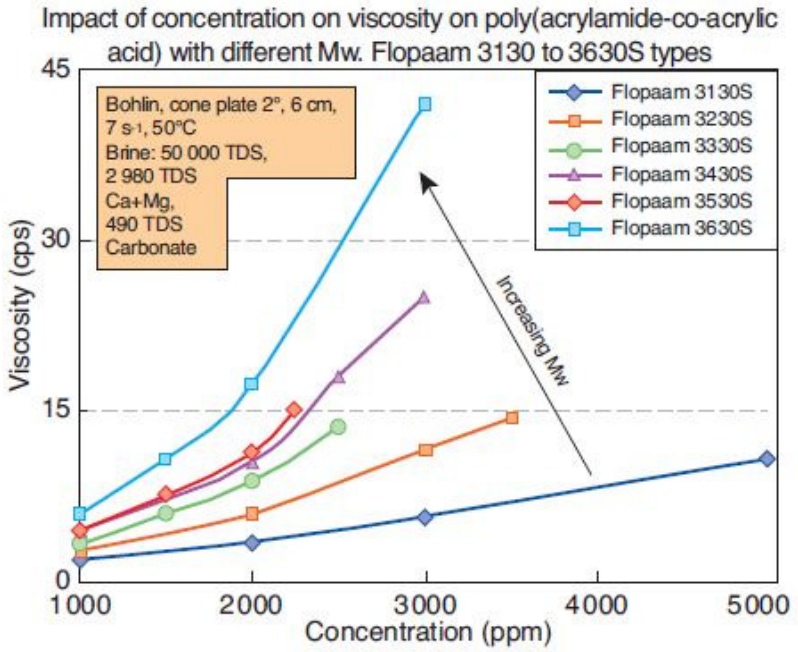

Figure 2-2 Effect of polymer concentration and moleculuar weight on solution viscosity[2].

2.2.1 Water flooding and polymer flooding

Flooding processes work by injecting water or polymer solutions through an injection well, thus creating a pressure support on the oil phase toward the production well and displacing the oil toward the producer. When the injected fluid move (sweep) through the reservoir some residual oil remains in place [1].

A typical polymer flooding strategy usually includes several different steps and fluids, often starting with a high concentration (and viscosity) polymer solution, and then reducing polymer concentration into the injection program. The “polymer” sweep front is then often followed by water injection or surfactant injection and then water injection. Figure 2-3 show a schematic of a typical surfactant / polymer /water EOR injection-production strategy [1].

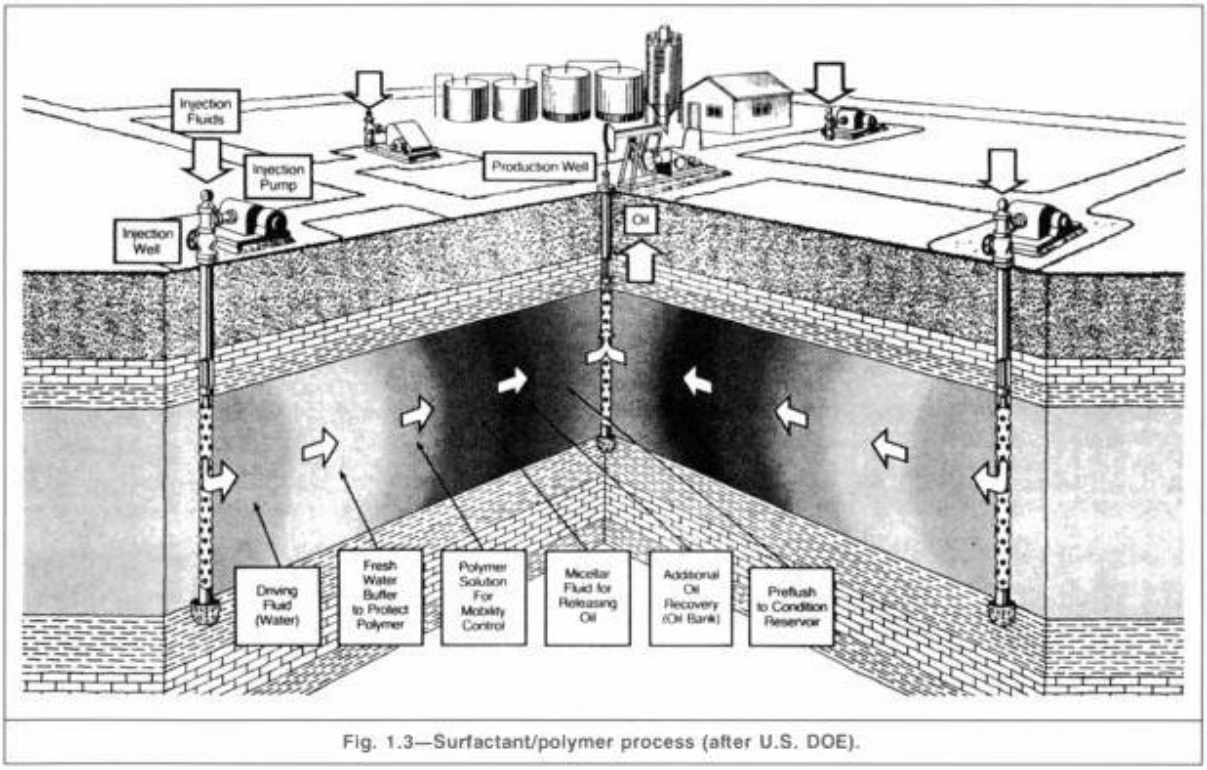

Fig. 1.3—Surfactant/polymer process (after U.S. DOE).

Figure 2-3 Schematic drawing of EOR by the use of waterflooding, surfactants and polymers [1]

One of the main reasons for using polymer injection as compared to a traditional water injection only is that of mobility control. If one define a mobility ratio as in eq.(2.1) where μ_o and μ_w represents the polymer and oil viscosity respectively and k represents the permeability for each phase, this is a measure of the ease of moving through the reservoir for the oil in relation to the displacing fluid (polymer or water) [1].

$$M = \frac{\mu_o / k_o}{\mu_w / k_w} \tag{2.1}$$

At high mobility ratios one will get problems of unstable displacement caused by viscous instabilities, known as viscous fingering, causing some of the oil in the reservoir to be bypassed by the sweep front. From eq. (2.1) it also becomes obvious why polymer floods can yield especially good results for viscous heavy oil reservoirs as they have an inherently unfavourable mobility ratio with water, and often require injection wells for production. The effect of viscous fingering and inhibition of viscous fingering through use of polymers is illustrated in Figure 2-4 [1].

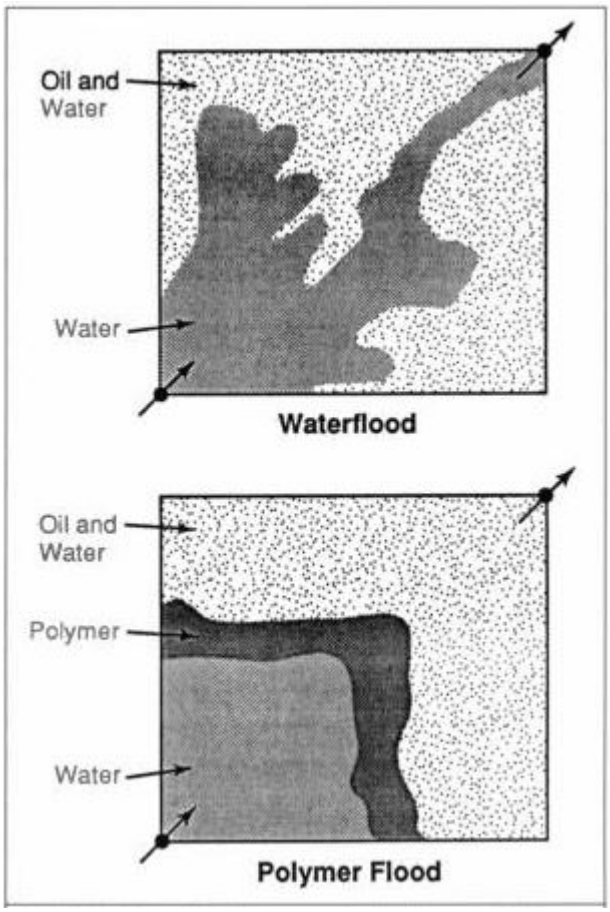

Figure 2-4 The reduction of viscous fingering and delayed water breakthrough during a polymer flooding process [1]

There are some studies claiming that polymer viscoelasticity may contribute to an increased sweep efficiency and reducing residual oil at the pore scale as compared to Newtonian fluids but there is some controversy as to whether this happens at real reservoir conditions or not [2].

2.3 Dimensionless groups

This chapter aims to introduce the most important dimensionless groups describing viscoelastic flow.

Perhaps the two most important groups in describing viscoelastic phenomena are the Weissenberg number (2.2) and Deborah number (2.3), the ratio of a fluid time constant to a characteristic time of flow. These two dimensionless groups are often the same, but not always. In this work (and usually in literature) the We number is defined as a fluid time constant λ multiplied with a deformation rate describing the flow, the deformation being the strain rate magnitude or maximum deformation rate $\dot{\gamma}$. The Deborah number is defined in the same way, a fluid time constant multiplied with a deformation rate, but here the deformation rate is usually the stretch rate $\dot{\varepsilon}$, often being transient in the fluid reference frame.

Weissenberg number:

$$\mathrm{We} = \lambda \dot{\gamma} \tag{2.2}$$

Deborah number:

$$\mathrm{De} = \lambda \dot{\varepsilon} \tag{2.3}$$

Another important dimensionless group for all flow is the Reynolds number (2.4), describing the ratio of inertial to viscous forces. In (2.4) ρ is density, v is velocity, D is some length scale of flow and μ is the dynamic viscosity.

Reynolds number:

$$\mathrm{Re} = \frac{\rho v D}{\mu} \tag{2.4}$$

For unsteady phenomena such as vortex shedding the Strouhal number (2.5) is often used as a dimensionless group describing the frequency of the unstable phenomena. In (2.5) L is some characteristic length scale and f is frequency.

Strouhal number:

$$\mathrm{St} = \frac{Lf}{v} \tag{2.5}$$

2.4 Polymer Rheology

When water or other "simple" Newtonian fluids are added even small amounts of a high molecular weight polymer its rheology (stress response to strain) may change dramatically. This subchapter will give a short and general introduction to the rheology of diluted polymer-water solutions. A more thorough introduction to models , strain rates and stresses is given in chapter 4.

The definition of a Newtonian fluid under simple shear is given in eq. (2.6) below

$$\tau \propto \frac{dv}{dx} \tag{2.6}$$

That is, the shear stress is proportional to shear rate, and this proportionality constant is what is commonly referred to as viscosity μ. Eq.(2.7)

$$\tau = \mu \frac{dv}{dx} \tag{2.7}$$

For fluids that are non-Newtonian this relation no longer holds. The proportionality constant (or viscosity) is dependent on the shear rate. Fluids where the proportionality increase with strain are known as dilatant or “shear thickening”. Fluids where the proportionality decrease with strain are known as Pseudo-plastic or “shear thinning”. Under normal steady shear HPAAM (and many other diluted polymer solutions) exhibit this behaviour [4]. Figure 2-5 shows the different modes of simple non-Newtonian shear dependent fluids [5].

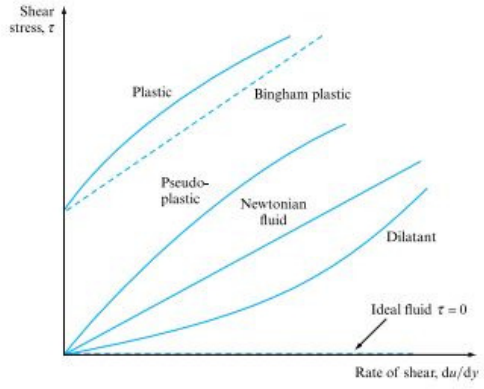

Figure 2-5 Shear stress vs shear rate for ideal, Newtonian and non-Newtonian fluids [5]

2.4.1 Shear thinning

The effect of shear thinning in polymer solutions is the result of polymer molecules orienting themselves in the flow field in a way that cause less resistance to deformation (viscosity) in a specific plane. The simplest and most common way to model this in polymers is by generalized Newtonian models. In these models the fluid is modelled as "Newtonian" with a shear rate dependent viscosity. One of the most common and simplest models is the Power-Law model where the viscosity is a power-law function of strain rate with the power law exponent n and a "zero shear viscosity" k (2.8). Many other generalized models exist, and the Careau Yasuda model that contains two "Newtonian plateaus" with power law behaviour between is the one that capture HPAAM bulk rheology most accurately. A further discussion on generalized Newtonian models is continued in Chapter 4.

$$\mu_{eff} = k\frac{dv}{dx}^{n-1} \tag{2.8}$$

From equation (2.8) and (2.7) the shear stress under simple shear for a power-law fluid can be shown to be (2.9)

$$\tau = k\frac{dv}{dx}^{n} \tag{2.9}$$

Solutions of HPAAM exhibits close to Newtonian behaviour at low concentration and/or molecular weight and shear thinning above some concentration and/or molecular weight. The viscosity is also largely dependent on ion concentration in the water. Typical HPAAM behaviour under simple shear can be seen in Figure 2-6[3] at different polymer molecular weights and hydrolysis with 1500ppm polymer in synthetic seawater (SSW). In Figure 2-6 the first number in the legend is the polymer molecular weight in 10^6 Daltons and the second is the percentage hydrolysis, ie. 20-30 is a $20*10^6$ Dalton polymer at 30% hydrolysis.

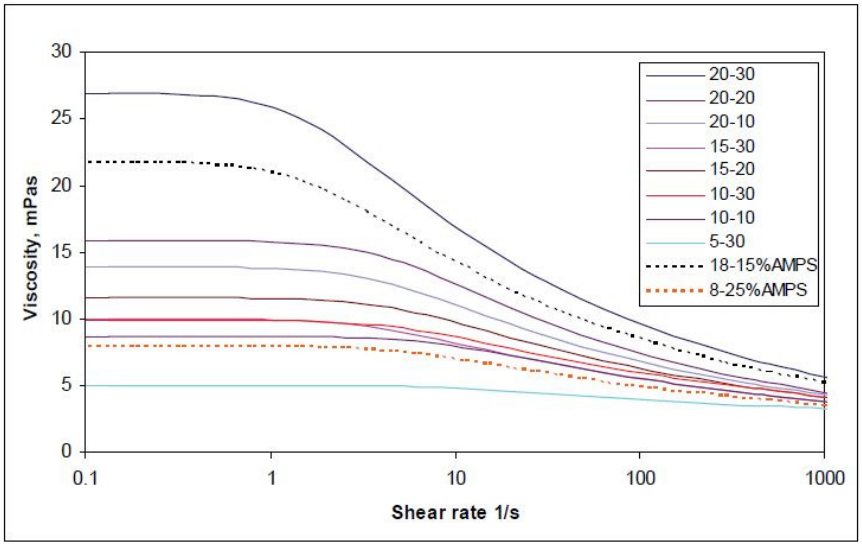

Figure 2-6 Shear thinning behaviour of HPAAM at different molecular weights and hydrolysis [3].

2.4.2 Increased apparent viscosity of HPAAM in porous media

When dilute polymer solutions such as HPAAM are flooded through porous media (as in EOR applications) some rather strange, (and still poorly understood) effect occurs. The resistance to flow, i.e. apparent viscosity increases dramatically with higher flow (and thus deformation) rate. This is the exact opposite of the shear thinning effect observed in bulk rheology measurements under simple shear. This effect also illustrates that the use of a simple shear thinning model and calculating some deformation rate from flow rate is not valid for flow in porous media [6].

The most common explanation is that when the diluted polymer solution enters a pore throat the extensional flow (stretch) causes the polymer molecules to uncoil, leading to a much higher apparent viscosity. This phenomena is named coil-stretch transition, and is something that has been thoroughly studied in polymer rheological societies, often with frustrating discrepancies in both computational and experimental results. The theory of having an "extensional viscosity" seems good in practice, and can explain the increase in apparent viscosity for porous media flows, but accurately measuring this fluid property in a consistent way has proven elusive [7].

Figure 2-7 shows results of measured extensional viscosity by different researchers on a test fluid known as the M1. This fluid is a Boger fluid, i.e. it has extensional properties, but its apparent bulk viscosity is independent of shear rate.

When considering that the results in Figure 2-7 is from different leading research groups, conducted on the same fluid, the problem of trying to accurately determine and define a "extensional viscosity" is evident. And thus the gathering of results below has by rheologists been ironically named "The M1 muddle". It is worth mentioning that all the results below are likely correct, it is the stress history due to different experimental methods that likely cause the discrepancies. 'The M1 muddle" is a good illustration that one has to be careful defining extensional viscosities, comparing experimental data and experiments and numerical simulations when working with "extensional" stretch thickening fluids [7].

> *"We reiterate the warning about extensional viscosity: it is fine in theory but is a very dangerous idea in practice, specifically when it is applied when steady flow has not been achieved."*
> *C. J. S. Petrie [7]*

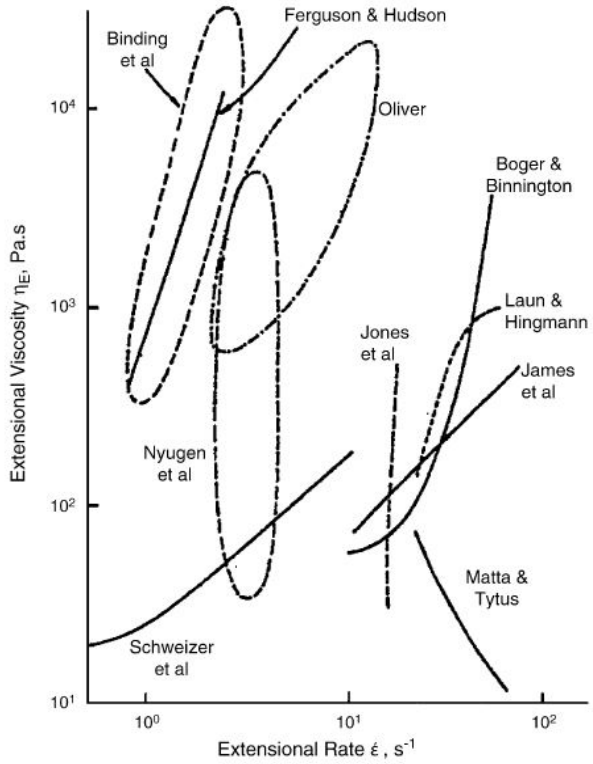

Figure 2-7 M1 muddle extensional viscosity [8]

3 Literature review

Although a lot of research has been conducted on HPAAM and viscoelastic fluids in general the interpretation of results vary. One of the challenges is that historically viscoelastic flow phenomena has been studied a lot in separate research disciplines, with different goals but ultimately studying the same viscoelastic effects. The flow of HPAAM in porous media has been studied experimentally and modelled empirically for decades in the oil industry due to the importance of understanding the fluid behaviour when used in reservoir flooding applications. HPAAM and polyacrylamide has been used a lot in more traditional rheological research as a "strange" viscoelastic fluid due to its high viscoelasticity and shear thinning. Traditional rheological research groups have also had a high focus on viscoelastc liquids in general the last decades as it is one of the phenomena that is the least understood, and with many real world applications. Last but not least visoelastic flow has been studied a lot in numerical computation and non-Newtonian CFD research and development, typically by mathematicians and physicists [4]. For this literature review, some articles from each of the different disciplines have been studied. The main reason for this is that even though the methods vary, the goal is ultimately the same; To understand viscoelastic flow phenomena in general and to make it possible to model the viscoelastic effects and make predictions based on numerical simulations.

3.1 Polymer Injectivity and mechanical degradation in porous media

Studies of the injectivity of HPAAM in porous media and mechanical degradation have been studied a lot in the oil-industry due to its real world applications. One of the largest problems when considering flow in porous media is that it is difficult to predict the rate of deformation for the fluid, i.e the shear and stretch rate. The most common way to quantify deformations is through various forms of the "capillary bundle" model or through empirical models. The capillary bundle model assumes that the porous media behaves as a capillary with the same pressure drop per length. For a capillary tube the shear rate for developed flow can be determined for Newtonian (or well defined) non-Newtonian fluids as this is one of the very few instances where the Navier Stokes equations has an analytic solution[9].

The use of the capillary bundle model and other empirical models also presents some challenges:

-Very often “fitting factors” are used.

-What model that is being used (and fitting factors) to predict shear rate is not consistent in literature.

-The theory that the increase in apparent viscosity is due to elongational flow is not consistent with the use of a capillary bundle model as this model per definition has no elongational flow.

The last point is usually solved by assuming that the stretch rate, (rate of elongation) is proportional to the shear rate in porous media, and the capillary bundle model is used. This approach has also lead to the fact that the increase in apparent viscosity in porous media is almost exclusively named “shear thickening” in typical oil-industry research, although most literature agree that the effect is indeed an extensional one, and not due to shear. The effect of increasing apparent viscosity is in rheological research and books usually named elongational, extensional or stretch thickening, terms that are clearer and more consistent with the actual phenomena. Some literature also uses the terms strain rate and shear rate for the same deformations, although shear deformation is only some of the components of the rate of strain tensor further described in Chapter.4 from more traditional continuum mechanics concepts.

Below are a collection of articles studying the injectivity and mechanical degradation of HPAAM in porous media and main conclusions. The different models used in these papers to calculate shear rate are presented in Table 3-1.

- In 1981 G. Chauveteau published the article given in [10]. The work is a systematic study of the extensional effects of HPAAM in different simple geometries, as well as in porous media. The article use a Careau Yasuda model to fit the shear thinning bulk viscosity, and the effect of increasing apparent viscosity in porous media is attributed to a coil stretch- transition effect occurring at a critical stretch rate determined by the polymer relaxation time. The article shows that it is possible to see the same increase in apparent viscosity as in porous media in simpler and more easily defined geometries, for instance in contractions and short capillary tubes.

- The 1984 article by K.S. Sorbie and L.J. Roberts [11] proposes a model for calculating injectivity characteristics (apparent viscosity) through a model based on polymer molecular weights, and a model for mechanical degradation. The model is based on a superposition of n pseudo components to calculate viscosity, and calculating degradation on each pseudo component as opposed to just using one average molecular weight. The increase in apparent viscosity (shear thickening) is explained by a extensional thickening /coil stretch transition effect. Mechanical degradation is attributed to "high strain flows", both extensional and shearing. Comparisons between the proposed model and experimental data show that the model can at least qualitatively explain both extensional thickening and molecular weight distribution/ viscosity after degradation.

- J.G. Southwick and C.W. Manke (1988) [12] studied Injectivity, mechanical degradation and elastic properties of HPAAM and Xantan in porous media and glass bead packs. The study also use a "ductless siphon" apparatus to measure the "extensional viscosity" of HPAAM, finding that the HPAAM solutions studied has an extensional viscosity more than a 1000 times higher than the bulk viscosity. The extensional viscosity found from the ductless siphon seems constant over a range of extension rates, consistent with finite extension nonlinear elastic "FENE" dumbbell models. The study shows that after mechanical degradation the decrease in extensional viscosity is far larger than the decrease in bulk viscosity. The decrease in extensional viscosity ("shear thickening") in porous media is not as high as the decrease observed in the ductless siphon. The magnitude of shear thickening in porous media was found to be dependent on the porous media permeability, but that the critical shear rate where it occurred was identical for geometrically identical porous media, ie. glass bead packing with different permeability.

- R. S Seright 2009 [13] studies the injectivity characteristics of the two EOR polymers HPAAM and Xanthan. It is shown that Xanthan does not exhibit the same increasing apparent viscosity in porous media as HPAAM. Xanthan is also shown to be more stable wrt. mechanical degradation.

- A. Stavland et.al 2010 [3] studied flow properties of HPAAM in porous media versus rheological properties. A large increase in apparent viscosity with flowrate in porous media is found, contrary to the shear thinning observed in bulk rheological measurements. The increase in apparent viscosity is attributed to elongational effects (coil stretch transition). A large systematic study of different polymer molecular weights and hydrolysis percentages are compared wrt. flow in porous media. Mechanical degradation is observed after a local maximum in apparent viscosity. It is shown that the critical shear rate where a increase in viscosity are observed is dependent on both molecular weight and hydrolysis. Further a modified Careau model is proposed capturing the increase in viscosity and decrease in viscosity due to mechanical degradation for porous media. The model does not have any transported quantities relating viscosity and mechanical degradation so that the fluid does not "change" after degradation such as in the model proposed by K.S. Sorbie and L.J. Roberts [11]. Mechanical degradation of the polymers are mainly attributed to excessive "stretching" in elongational flows.

- D.G Hatzignatiou, H. Moradi and A.Stavland 2013 [6] study flow of HPAAM through both porous media and capillary tubes, showing that an increase in apparent viscosity is observed in capillary tubes with a length/radius ratio of 3150. An increase in apparent viscosity for HPAAM in porous media is found.

Table 3-1 Models for shear and elongation rate in porous media used in literature studied

Author	Calculation of shear rate	Calculation of elongation rate
G. Chauveteau (1981) [10]	$\dot{\gamma} = \alpha \frac{4v}{\sqrt{8\frac{k}{\phi}}}$ $\alpha = 1.7$ (Beads)	$\frac{\dot{\varepsilon}}{\dot{\gamma}} \approx 0.4$
K.S. Sorbie and L.J. Roberts (1984) [11]	$\dot{\gamma} = \beta \frac{v}{\sqrt{k\phi}}$	$\dot{\varepsilon} = \frac{v}{d_p}$
J.G. Southwick and C.W. Manke (1988) [12]	$\dot{\gamma} = \frac{v}{\sqrt{k}}$	$\dot{\varepsilon} = \frac{2v}{d_p}$
R. S Seright (2009) [13]	Results plotted against flow rate only	(-)
A. Stavland et.al 2010 [3]	$\dot{\gamma} = \alpha \frac{4v}{\sqrt{8\frac{k}{\phi}}}$ $\alpha = 2.5$	$\dot{\varepsilon} = \frac{2v}{d_p}$
D.G Hatzignatiou, H. Moradi and A.Stavland (2013)	$\dot{\gamma} = \alpha \frac{4v}{\sqrt{8k\phi}}$	(-)

For all formulas in Table 3-1:

$\dot{\gamma}$ = apparent shear rate

v = Darcy velocity

k = Permeability

ϕ = Porosity

β , α = Shape factors/fitting factors

As well as the models for deformation rates given in Table 3-1, the book chapter in [9] give a comprehensive list of models for shear rate in porous media, as well what assumptions they are derived from. The table of models from the book is given in its original form in Table 3-2.

Table 3-2 Mathematical models for calculation of apparent shear rate in porous media [9]

No.	Equations	Prerequisite conditions and Assumptions	Source
1	$\gamma_{app} = \frac{4u}{\phi r} \cdot \frac{L_e}{L}$ (7) where u is the superficial flow rate, *cm/s*; ϕ is porosity; r is the average pore radius, *cm*; L_e is length of tortuous flow path, *cm*; L is the porous media length, *cm*;	1. Porous media is considered as a bundle of capillary tubes with a length that is greater than the porous media by a tortuous factor; 2. Bundle of straight capillaries; 3. Capillaries are of uniform sized; 4. Capillaries are not interconnected; 5. Flow rate in capillary is constant (at constant pressure drop).	(Kozeny 1927) (Carman 1937)
2	$\gamma_{app} = \left(\frac{3n+1}{4n}\right)\frac{12G}{\rho\sqrt{150k\phi}}$ (8) where n is the Power law parameter; ρ is fluid density, *g/cm³*; k is permeability, *cm²*; ϕ is porosity; G is mass velocity, *g/(cm² sec)* $G = \rho\left(\frac{k}{H}\frac{\Delta P}{L}\right)^{1/n}$ (9) where ΔP is the pressure drop, *dyne/cm²*; k is permeability measured by a Newtonian fluid, *cm²*; L is the unit length, *cm*; H is the non-Newtonian bed factor, *dyne sec^n cm^{-1-n}* $H = \frac{K}{12}(9+3/n)^n(150k\varphi)^{(1-n)/2}$ (10) where K is the Power law parameter, *dyne sec^n cm^{-2}*	The permeability of the porous media is the same for all identical packed bed configurations, independent of flow conditions in the bed.	(Christopher and Middleman 1965)
3	$\gamma_{app} = \left(\frac{3n+1}{4n}\right)^{n/(n-1)}\frac{12u}{\sqrt{150k_p\phi_w}}$ (11) where n is the bulk power law index; u is the	1. Based on capillary bundle model for non-Newtonian fluid flow; 2. The polymers such as partially hydrolyzed	(Hirasaki and Pope 1974)

	Darcy velocity, *cm/s*; k_p is polymer permeability, cm^2; Φ is porosity; Φ_w is the pore space occupied by water, $\Phi_w = \Phi S_w$	polyacrylamides, the permeability reduction due to the adsorption of the polymer is considered; 3. When applied to Xanthan biopolymer through rock cores (at residual oil), very good agreement was obtained between calculated and experimental values; 4. A tortuosity of 25/12 has been assumed.	
4	$$\gamma_{app} = C\left(\frac{3n+1}{4n}\right)^{n/(n-1)} \frac{u}{\sqrt{k_w S_w \phi}} \quad (12)$$ where k_w is water permeability, cm^2; S_w is water saturation; n is the bulk power law index; C is shear rate coefficient, not constant, but a function of the network parameters; ϕ is porosity; u is Darcy velocity, $u=Q/A$, *cm/s*;	Equation is developed to relate the flow of Xanthan solutions in cores having different permeabilities, lithologies, and oil saturations.	(Cannella, Huh et al. 1988)
5	The average pore radius in the pack is estimated from the capillary bundle model of the porous medium. The equation: $$r = \left(\frac{8k}{\varphi}\right)^{1/2} \quad (13)$$ is shown to give a good estimate of the average hydrodynamic pore radius in homogeneous unconsolidated porous media. The equation for the shear rate at the pore wall in such media is taken as: $$\dot{\gamma} = \alpha \frac{4v}{r} \quad (14)$$ Where k is permeability, cm^2; ϕ is porosity; a is a shape parameter characteristic of the pore structure, a=1.7 for packs of large spheres having same diameter, a=2.5 for packed beds of angular grains; v is the superficial velocity, *cm/s*; r is the average pore radius, *cm*;	1. Calibrated glass beads having different diameters are packed to conduct experiments; 2. The porous media is assumed to have similar pore shapes but different pore sizes. 3. The shear rate is a maximum wall shear rate in the average pore throat diameter.	(Chauveteau and Zaitoun 1981) (Zitha, Chauveteau et al. 1995)

3.2 Polymer rheometry

There has been many developments in equipment for measuring extensional rheology the last 10-20 yrs. Traditionally viscoelasticity has been measured in “normal” cone and plate rheometers with small amplitude oscillatory shear. Recent advances show that this method, even tough able to measure viscoelastic phenomena can not capture the effects observed in highly elongational flows such as coil stretch transition in diluted polymer solutions [4]. There exists some instruments made for quantitatively measuring extensional properties, namely the ductless siphon, spinning rheometer, Capillary Breakup Extensional Rheometer (CaBER) and Filament Stretching Extensional Rheometer (FiSER), as well as other approaches with opposing nozzles, opposing jets and so on. The number of different techniques, and fast development in instruments for these measurements indicate that the experimental techniques are far from fully developed, something the “M1 muddle” in Figure 2-7 also shows. In this subchapter some papers studying extensional viscosity in some traditional ways i.e small amplitude oscillatory cone and plate as well as more novel techniques are reviewed with main points and conclusions.

- In the 1999 paper by G. H. McKinley et al [14], the uniaxial elongation of a set of ideal elastic fluids compromised of a dilute concentration of linear polystyrene chains in styrene are studied. The technique used is a Filament Stretching Extensional Rheometer (FiSER). It is found that over a critical Deborah number the extensional strain (and viscosity) increase rapidly up to a steady state value corresponding to full elongation of the polymers. This response is what is predicted by finite extension viscoelastic models. It is found that the FiSER provides a mean of probing the stress growth in viscoelastic fluids during transient uniaxial extension. A series of instabilities are also observed in the FiSER, including filament failure. These instabilities are poorly understood, and can possibly shed new light on other poorly understood phenomena in viscoelastic liquids.

- In a 2000 Master Thesis by Ali Kreiba [15] the shear response, elastic response and dynamic behaviour of high concentration 1-5% Polyacrylamide solutions are studied using a cone and plate rheometer. The work found that polyacrylamide is not only shear thinning, but different modes of thixotropy was also observed in dynamic experiments.

This means that the shear thinning has a dynamic behaviour that is measurable, such that the thinning under shear is not “instantaneous”. Elastic behaviour was studied using oscillatory shear.

- A. Bhardwaj et. al. 2007 use a Filament Stretching Extensional Rheometer (FiSER) and a Capillary Breakup Extensional Rheometer (CaBER) [16]to measure the extensional behaviour of “wormlike” micellar solutions. It is found that the extensional viscosity measured by CaBER and FiSER are one order of magnitude different. This illustrates the difficulties of trying to assess extensional viscosity as a fluid property, and the discrepancies between the two methods are attributed to the different dynamics of the extensional flow. This discrepancy also brings into question the viability of using capillary breakup experiments to accurately measure extensional viscosity. A very interesting effect observed in the experiments, and one that may shed some light on HPAAM degradation processes is the catastrophic failure of the filament at some extension rate. This is attributed to the scission of the molecule chains due to excessive stretching.

- In a 2011 Ph.D thesis A. Lanzaro [17] studies micro fluidic flow of PAAM in well defined geometries using pressure measurements as well as micro-particle image velocimetry. The polymers used are also characterized using gel-permeation chromatography (GPC) for mole-weight distributions. The polymer solutions rheology is studied using a Couette rheometer under both steady shear and oscillatory shear as well as with a high frequency squeeze flow rheometer and with a capillary breakup (CaBER) rheometer. It is found that the effect on the flow field in the microfluidic device is highly influenced by viscoelasticity. A methodology for evaluating stretch rates using image based particle velocimetry in the microfluidic device is presented. Further work on developing microfluidic rheometers with both steady and oscillatory flow show promise as a way of quantifying extensional properties. The approach of image based particle velocimetry also show promise as a method for quantifying the actual stretch rates in a complex flow geometries, and coupled with pressure measurements might shed light on effects such as coil stretch transition.

In general it seems that the rheometric approaches presented above may show promise in quantifying and predicting extensional flow properties of HPAAM in porous media. Still large discrepancies in measurements are observed for different rheometer principles and thus the development of a consistent and accurate measurement principle is still a work in

progress. The observed filament breakup attributed to molecule scission in extensional rheometers show promise for studying HPAAM mechanical degradation in extensional flows.

3.3 CFD modeling of viscoelatic fluids

Simulating viscoelastic flows using CFD codes have been a long standing goal in non-Newtonian numerical fluid mechanics. The frameworks for constitutive models were largely developed around the 1940-50's, from a convected derivative formulation of the linear viscoelastic Maxwell material proposed by James Clerk Maxwell in 1867.[4] [18] The first work on numerical solutions of non-Newtonian flow problems started in the early 1970's. The main problem in CFD simulations of viscoelastic fluids since then has been numerical stability, and what is known as "the high Weissenberg problem". A lot of work on discretization schemes, stabilization procedures and algorithms has lead to CFD codes running viscoelastic constitutive equations at higher Weissenberg and Deborah numbers then possible in the 70's and 80's, but numerical stability is still one of the main issues with viscoelastic CFD codes [18]. This chapter aims to review some of the current work on CFD simulations of viscoelastic fluids, and its applicability at understanding and predicting experimental effects in flows of dilute HPAAM solutions.

- P.J Oliveira (2001) [19] presents a custom written finite-volume method for transient simulations of viscoelatic flows. The geometry and phenomena studied are vortex-shedding effects behind a cylinder. The constitutive model used are a variation of the FENE-CR model that has a constant shear viscosity and a bounded extensional viscosity. The numerical model shows a tendency to suppress vortex formation behind the cylinder, and that the Strouhal number (and thus vortex shedding frequency) are reduced with a viscoelastic model compared to a Newtonian model. The drag on the cylinder is also reduced in calculations using a viscoelastic model.

- G. N. Rochaa, R. J. Pooleb et al. (2008) [20] Studies extensibility effect in the cross-slot flow bifurcation using the FENE-P and FENE-CR models using a finite-volume method. The motivation is the effect that flexible polymer solutions have shown to develop a instability and unsymmetrical flow in this geometry not observed for Newtonian fluids. The experimental study that motivated this work used a polyacrylamide (PAAM) solution to study this effect. The study shows that numerical

simulations are able to capture this instability effect and are in qualitative agreement with the experimental study using polyacrylamide.

- A.M. Afonso, P.J Oliveira et al. (2011)[21] studies the dynamics of viscoelastic entrance flow. The study are mainly focused on a 4:1 abrupt contraction geometry often used as a 2D-benchmark case for viscoelastic equations. The study used the Oldroyd-B and PTT (Phan-Thien & Tanner) models as constitutive equations as well as a log-conformation tensor approach for high Deborah numbers. Experimentally these abrupt contraction geometries have shown that viscoelastic fluids have a influence on the vortexes present in this geometry. This geometry also shows the effect of "coil-stretch transition" and increased apparent viscosity/ inlet pressure loss in experimental studies. The effect of higher pressure drops then for a Newtonian fluid was not captured by the simulations. It was found that the log-conformation tensor approach are able to converge for much higher Deborah numbers than the standard approach with an extra transported stress tensor which was found to diverge at a low critical Deborah number.

- H.R Tamaddon-Jahromi, M.F. Webster and K. Walters paper from 2010 [22] focus on numerically predicting the large increases in extra pressure drops with Boger fluids in axisymmetric contractions. Even tough this phenomena has been observed experimentally, replicating this result has proven frustratingly difficult in numerical simulations, even qualitatively. The study use the Oldroyd-B model, White-Metzner model, an Inealstic model and a FENE-CR model to study the pressure drop compared to a Newtonian fluid over a contraction-expansion geometry. It is found that the FENE-CR model are able to qualitatively capture the increased pressure loss in numerical simulations. The extra pressure loss is still a lot lower than what has been observed experimentally.

- A. Afsharpoor et al. (2012) [23] uses the commercial CFD software ANSYS-Polyflow to study the effect of polymer elasticity on residual oil saturation at the pore-scale. The constitutive model used is the Oldroyd-B model. It is found that "extra" normal stress forces acts on static oil droplets at the pore scale level with viscoelastic fluids. These normal stresses are insignificant for Newtonian fluids.

Even though a lot of advances has been done in CFD studies of viscoelastic flow over the last two decades, viscoelastic simulations are still plagued by numerical instabilies and convergence issues. Further still the effect of an increased pressure drop (apparent viscosity) in extensional flow/entrance geometries has proved frustratingly difficult to achieve numerically even though it is observed in numerous experimental studies. The use of viscoelastic models show promise in understanding drag reduction and influence on turbulence and vortex mechanisms but a lot more research is still required.

The effect of increased apparent viscosity in porous media for HPAAM, usually attributed to “extensional viscosity” under elongational flow in pore entrances has still not been consistently achieved numerically, even qualitatively.

4 Continuum mechanics description of flow

The core idea in fluid mechanics and CFD in general is that the fluid studied can be considered a continuum. That is, at the scale studied the fluid acts as a continuous substance and not discrete particles. This chapter aims to give a brief introduction to the continuum mechanics equations describing fluid flow. For more in depth derivations of some of the concepts the reader is referred to the books given in [4, 5, 18, 24].

In general, a flowing fluid can be described by 4 partial differential equations and one equation of state (EOS) in 3D space if energy and nuclear reactions is neglected and the fluid is considered a continuum. That is conservation of mass (4.1), and the conservation of momentum in x- (4.2) y-(4.3) and z-direction(4.4) and an equation of state, for instance the ideal gas law. For the problems considered later in this chapter the fluid is considered incompressible such that a EOS is not needed.

$$\frac{\partial \rho}{\partial t} + \mathrm{div}(\rho \vec{u}) = 0 \tag{4.1}$$

$$\frac{\partial \rho u}{\partial t} + \mathrm{div}(\rho u \vec{u}) = -\frac{\partial P}{\partial x} + \frac{\partial \tau_{xx}}{\partial x} + \frac{\partial \tau_{yx}}{\partial y} + \frac{\partial \tau_{zx}}{\partial z} + S_x \tag{4.2}$$

$$\frac{\partial \rho v}{\partial t} + \mathrm{div}(\rho v \vec{u}) = -\frac{\partial P}{\partial y} + \frac{\partial \tau_{xy}}{\partial x} + \frac{\partial \tau_{yy}}{\partial y} + \frac{\partial \tau_{zy}}{\partial z} + S_y \tag{4.3}$$

$$\frac{\partial \rho w}{\partial t} + \mathrm{div}(\rho w \vec{u}) = -\frac{\partial P}{\partial z} + \frac{\partial \tau_{xz}}{\partial x} + \frac{\partial \tau_{yz}}{\partial y} + \frac{\partial \tau_{zz}}{\partial z} + S_z \tag{4.4}$$

In the above equations u, v and w represents the velocity components in x, y and z directions respectively (unknowns), $\vec{u}$ is the velocity vector, ρ is density (constant), P is pressure (unknown) and τ_{ij} is the stresses introduced by deformation of the fluid. S represents "other" sources in the momentum equations, such as body forces. If "other sources" is zero and density is considered constant the above equations has 4 unknowns (+9! unknown stresses).

For the system of PDE's above to be solved a closure relating the stresses to known quantities has to be introduced. The most common of these closures is the one of Newtonian fluids, that is, stress is proportional to deformation.

4.1 Viscous stresses

As stresses are of great importance when studying typical polymer-diluent systems such as HPAAM, and that a lot of the "strange" effects in this fluid is attributed to fluid stresses a more thorough introduction into fluid stresses is given here. For simplicity the case of 2D is considered as this introduces 4 instead of 9 stress components. For each direction (x and y) there are two stress components.

x-direction

τ_{xx} - Stresses acting on the fluid element in the x direction due to deformations (changing u velocity) in the x direction (ie. Stretching of the fluid)

τ_{yx} - Stresses acting on the fluid element in the x direction due to deformations (changing u velocity) in the y direction (ie. Shearing of the fluid element)

y-direction

τ_{xy} Stresses acting on the fluid element in the y direction due to deformations (changing v velocity) in the x direction (ie. Shearing of the fluid element)

τ_{yy} Stresses acting on the fluid element in the y direction due to deformations (changing v velocity) in the y direction (ie. Stretching of the fluid)

For a Newtonian fluid the following assumptions are introduced:

1. The stress is zero when fluid is not moving
2. The stress is proportional to deformation
3. The proportionality between deformation and stress is isotropic
   (that is the fluid has no "preferred" plane of deformation)

Through some derivation and the above assumptions the stresses in a Newtonian fluid can be shown to be (4.5)(4.6) and (4.7):

$$\tau_{xx} = 2\mu \frac{\partial u}{\partial x} \tag{4.5}$$

$$\tau_{xy} = \tau_{yx} = \mu(\frac{\partial u}{\partial y} + \frac{\partial v}{\partial x}) \tag{4.6}$$

$$\tau_{yy} = 2\mu\frac{\partial v}{\partial y} \tag{4.7}$$

4.2 Non Newtonian rheological models

For many real fluids and especially polymer systems the assumptions in the Newtonian fluid simplification does not hold in reality. The fluid may exhibit "yield stress" such that assumption 1 is not valid. The fluid may exhibit thickening or thinning when deformed such that assumption 2 is not valid. The fluid may have molecular effects such as molecules stretching and aligning in the flow field such that assumption 3 is not valid. For complex rheological fluids such as HPAAM the fluid actually exhibit all these three non-Newtonian effects.

The most common "problem" with simulating non-Newtonian fluids traditionally is the effect of strain thinning or thickening. This is usually solved trough "Generalized Newtonian models", that is the proportionality μ is some function of deformation rate. A large variety of these models exists, and they are simple to fit to rheological data. One of the simplest is the power-law model introduced in chapter 2, given in eq (4.8) where $\dot{\gamma}$ is the strain rate magnitude, μ_0 is the zero shear viscosity and n is the power law constant. For n<1 the fluid is shear thinning and n>1 the fluid is shear thickening.

$$\mu_{eff} = \mu_0 \dot{\gamma}^{n-1} \tag{4.8}$$

Another common model found to fit well for HPAAM under shear [3] is the Carreu-Yasuda model given in eq.(4.9) [4] where μ_∞ is the infinite shear viscosity λ is a time constant and a is a dimensionless parameter describing the transition from the zero shear to the power law viscosity. In effect the Carreau-Yasuda model is a power-law model, tying together two "Newtonian" viscosity plateaus at high and low shear.

$$\mu_{eff} = \mu_\infty + (\mu_0 - \mu_\infty)[1 + (\lambda\dot{\gamma})^a]^{\frac{n-1}{a}} \tag{4.9}$$

Even though the generalized Newtonian models are good at describing certain flows and fluids they also have some limitations. The change in fluid effective viscosity is "instantaneous" under strain. Another simplification that may lead to discrepancies during simulations is the fact that the generalized Newtonian models still consider viscosity an isotropic scalar. That is, the viscosity in all deformation planes is equal. The fact that the strain rate magnitude is used for calculating effective viscosity in the above models in for instance ANSYS Fluent [25], leads to stretch of the fluid contributing to an extensional "strain" thinning, such that the extensional viscosity is reduced in a shear thinning fluid. This is something that is opposite of the effect of coil stretch transition observed in flexible polymers experimentally. This also illustrates that care must be taken when fitting generalized Newtonian models to rheometric data that are collected under shear only, and then used when simulating complex flows for diluted polymer systems.

4.3 Viscoelastic constitutive models

The effects of elasticity, dynamics of strain thinning, extensional viscosity etc. can theoretically be captured in CFD simulations but it will require a more complicated closure to the momentum equations than the Newtonian or generalized Newtonian models. A common and simple linear model for elastic fluids is the one proposed by Maxwell in 1864. The model that was proposed to explain fluids with both viscosity and elasticity is that of eq.(4.10) [4] where G is an elastic modulus. The model proposed by Maxwell can be visualised as the fluid acting as a damper and spring connected in series. Fast (wrt. to the system time constant) dynamic changes influence the "spring" i.e elasticity only and slow dynamic changes influence the damper "viscous forces".

$$\tau_{yx} + \frac{\mu}{G}\frac{\partial \tau_{yx}}{\partial t} = \mu \dot{\gamma}_{yx} \tag{4.10}$$

The Maxwell model is only applicable when considering systems with small displacements. For a more general model (that can be used in CFD) the derivative in (4.10) has to be convected. A model proposed by Oldroyd is that of the Upper Convected Maxwell (UCM) model given in eq. (4.11) [4] in which $\overset{\nabla}{T}$ is the upper convected derivative ("Oldroyd derivative") of the stress tensor defined in eq. (4.12)

$$T + \lambda \overset{\nabla}{T} = \mu \dot{\gamma} \tag{4.11}$$

$$\overset{\nabla}{A}_{ij} = \frac{\partial}{\partial t} A_{ij} + v_k \frac{\partial A_{ij}}{\partial x_k} - A_{kj} \frac{\partial v_i}{\partial x_k} - A_{ik} \frac{\partial v_j}{\partial x_k} \tag{4.12}$$

Another commonly used viscoelastic model proposed by Oldroyd is the Oldroyd B model given in eq. (4.13). If the second time constant λ_2 is zero then the Oldroyd B model reduces to the UCM model.[18]

$$T + \lambda_1 \overset{\nabla}{T} = \mu_0 (\dot{\gamma} + \lambda_2 \overset{\nabla}{\dot{\gamma}}) \tag{4.13}$$

The Oldroyd B model is commonly rewritten as a sum of solvent stresses and polymeric stresses, giving the model of eq.(4.14)(4.15) [18]

$$T_{ij} = \mu_s \dot{\gamma}_{ij} + \tau_{pij} \tag{4.14}$$

$$\tau_p + \lambda_1 \overset{\nabla}{\tau}_p = \mu_p \dot{\gamma} \tag{4.15}$$

Here μ_s and μ_p are the solvent and polymeric viscosities respectively such that $\mu_0 = \mu_s + \mu_p$ and $\mu_s = \frac{\lambda_2}{\lambda_1}\mu_0$, $\mu_p = (1 - \frac{\lambda_2}{\lambda_1})\mu_0$.

The Oldroyd B and UCM models does not act shear thinning, but contain elastic phenomena. Another limitation with the two above models is that when extension approaches a critical rate, that is $De = \frac{du}{dx}\lambda_1 = 0.5$ the ”extensional viscosity” is infinite. Different models have been suggested to more accurately capture the real behaviour of polymeric liquids, for instance the White-Metzner model, an Oldroyd B model where the polymer viscosity is modelled using a Generalized Newtonian model, for instance Power Law (4.8) or Carreau Yasuda (4.9).

A class of models trying to capture the real physics of polymer systems more accurately are the Finite Extension Non-linear Elastic (FENE) family of models. In these models the “spring constant” of the UCM and Oldroyd B models are nonlinear, such that extensional viscosity is bounded and has a finite value for “maximum extension”. Some of these models also contain some interesting phenomena, such as the FENE-P model that are derived from physics but capture not only elastic phenomena, but shear thinning and shear thinning dynamics as

well.[4] As the viscoelastic CFD simulations were mainly done using a Oldroyd-B model, the other models are not covered in detail here.

The models behaviour does shed some light on the issue of numerical stability often encountered in simulations. For instance the UCM and Oldroyd models have infinite extensional viscosity above a critical Deborah number, such that the complete numerical breakdown of simulations at these Deborah numbers are expected.

4.4 The Haagen Pouisulle equation for capillary flow

As the equation for capillary flow known as the Haagen Pouisulle equation is relevant for capillary viscosity measurements the equation is derived here from the Navier Stokes equations. The Haagen Pouisulle equation is one (of very few) analytical solutions to the Navier Stokes equations.[5, 24]

The Haagen Pouisulle equation makes the following assumptions:

1. Steady and laminar flow (d/dt=0)
2. No radial flow and no swirling flow
3. Axisymmetric fully developed flow
4. Incompressible fluid
5. Newtonian fluid

From the above assumptions, the equations of continuity and conservation of momentum written in cylindrical coordinates reduce to eq.(4.16)

$$\frac{1}{r}\frac{\partial}{\partial r}\left(r\frac{\partial u_z}{\partial r}\right)=\frac{1}{\mu}\frac{\partial P}{\partial z} \tag{4.16}$$

Through integration eq (4.16) has an analytical solution:

$$\int \partial\left(r\frac{\partial u_z}{\partial r}\right)=\int \frac{1}{\mu}\frac{\partial P}{\partial z} r\partial r$$

$$r\frac{\partial u_z}{\partial r}=\frac{1}{2\mu}\frac{\partial P}{\partial z}r^2+C_1$$

$$\int \partial u_z = \int (\frac{1}{2\mu}\frac{\partial P}{\partial z} r + \frac{C_1}{r})\partial r$$

$$u_z = \frac{1}{4\mu}\frac{\partial P}{\partial z} r^2 + C_1 \ln(r) + C_2$$

The integration constants C1 and C2 can be found through the following two boundary conditions:

Finite velocity u_z at the axis r=0 $\Rightarrow C_1 = 0$

No slip wall, $u_z = 0, r = R \Rightarrow C_2 = -\frac{1}{4\mu}\frac{\partial P}{\partial z} R^2$

When the boundary conditions are applied the parabolic velocity profile of laminar axisymmetric flow is achieved in eq.(4.17) with the maximum velocity at r=0 given in eq.(4.18)

$$u_z = -\frac{1}{4\mu}\frac{\partial P}{\partial z}(R^2 - r^2) \tag{4.17}$$

$$u_{z\max} = u_z = -\frac{1}{4\mu}\frac{\partial P}{\partial z} R^2 \tag{4.18}$$

Integrating eq (4.17) over the pipe cross section yield the average velocity in eq.(4.19)

$$u_{zavg} = \frac{1}{\pi R^2}\int_0^R -\frac{1}{4\mu}\frac{\partial P}{\partial z}(R^2 - r^2) 2\pi r dr = -\frac{1}{8\mu}\frac{\partial P}{\partial z} R^2 = 0.5 u_{z\max} \tag{4.19}$$

Assuming linear pressure drop along the pipe $-\frac{\partial P}{\partial z} = \frac{\Delta P}{L}$ and combining with (4.19) give the Haagen Pouisulle equation (4.20).

$$\Delta P = \frac{8 u_{zavg} \mu L}{R^2} \tag{4.20}$$

Through the above derivations the shear rate in capillary flow can also be found from eq.(4.21)

$$\frac{\partial u_z}{\partial r} = \frac{1}{2\mu}\frac{\partial P}{\partial z} r \tag{4.21}$$

Where the maximum shear rate is given in eq. (4.22), achieved by combining (4.21) and (4.20):

$$\left.\frac{\partial u_z}{\partial r}\right|_{Max} = \left.\frac{\partial u_z}{\partial r}\right|_{Wall} = \frac{4u_{zavg}}{R} \tag{4.22}$$

5 Experimental work

To study the effect of shear thinning and increase in apparent viscosity encountered in porous media, experimental work was done on the flow of HPAAM in capillary tubes at various lengths. The choice of tubing, tubing lengths and polymer was motivated by the following:

- If the increase in apparent viscosity in porous media is an elongational effect this effect should be visible for flow in short capillary pipes. If the apparent viscosity is calculated from pressure drop in capillary pipes of various lengths through the Haagen Pouisulle equation, without considering inlet effects, then short capillary tubes should give a higher apparent viscosity than long tubes. If this is observed then the "thickening" is indeed an inlet effect and not an increase in viscosity at high shear rates.
- To achieve shear rates as high as those that may be encountered in porous media then a small tube diameter is required to achieve high Deborah and Weissenberg numbers while still maintaining laminar flow.
- All experimental runs should aim to be in the laminar flow regime, the main goal is to study elongational inlet effects, not turbulent flow and polymer drag reduction.
- Two concentrations of FLOPAAM 3630s was chosen, 600ppm and 1500ppm at close to SSW salinity, this was motivated by the following:
    - FLOPAAM 3630s is a common EOR polymer, and has a high mean molecular weight of about 18 million Daltons. High molecular weight means longer molecules, which in turn should lead to larger extensional effects.
    - Rheological data for these solutions are known[1] through work at International Research Institute of Stavanger (IRIS)

[1] Report received from Statoil, "Viscosity of FLOPAAM 3630s at different dilutions in synthetic seawater (SSW)", International Research Institute of Stavanger.

- When close to Synthetic Seawater (SSW) salinity (0.75 SSW and upwards) the salt content does not change viscosity much.
- At high salinity (SSW) the bulk viscosity of the solutions are “low”, but extensional effects should still be very much present, this should make the inlet effects more visible as they are not “masked” by high bulk viscosity.

5.1 Chemicals and polymer solution preparation

The two solutions used were prepared from a stock 1% solution prepared by SNF and received from Statoil.

The composition of the stock solution was as following:

1% FLOPAAM 3630s in water
4.04% NaCl
0.55% $CaCl_2$

The solutions was prepared through volumetric methods instead of weight. This was motivated by the fact that all solutions used are very close to 1kg/l due to their low concentration of salts and polymer. Volumetric methods were chosen as they are fast and simple. As the main motivation is studying the extensional effects and not a very accurate characterization through a rheometric device, the sources of error in the experimental apparatus are likely higher than the errors introduced through the solution preparation.

Both nitrogen purging and degassed solvent as well as no special oxygen precautions were tried. The solutions with no special oxygen precautions appeared stable over the timeframe experiments were done (2days) but changed behaviour over 1week+. The solutions that was prepared from degassed solvent and with nitrogen purging appeared to be stable over a 1week+ timeframe, and it was this approach that was used for most solutions. The procedure for preparing the solutions was as following:

1. 20g of lab grade (99.5%) NaCl was measured up and 1L NaCl solution was prepared using distilled water to give a 20g/l brine.
2. The brine was degassed under vacuum for at least 20mins until most dissolved gas was released (observed by bubbles not appearing in solution under low pressure).

3. The polymer stock solution was measured up using a measurement cylinder, a 100mL cylinder was used for the 60ml for 600ppm solution. 200mL cylinder for the 150mL for the 1500ppm solution. The same measurement cylinders were used every time a new solution was prepared. After measuring out the stock polymer the bottle of stock polymer was immediately purged with nitrogen.
4. The polymer was transferred from the measurement cylinder to a 1000mL measurement cylinder and the polymer measurement cylinder was rinsed with the prepared degassed brine at least 4 times.
5. The 1000mL cylinder was topped off with the degassed brine and then the whole volume was transferred to a 1L plastic bottle.
6. The 1L plastic bottle was purged with Nitrogen before it was closed.
7. The solution in the plastic bottle was stirred gently and left to set for at least 24hrs before use.

The pH of the solutions was checked with indicator paper and found to be in the range 6-7, such that no further pH adjustments was done.

The stock solution did contain some contaminants which was also observed in the prepared solutions. Due to risk of mechanical degradation the prepared solutions was not filtered. When left to set it became apparent that the contaminant particles were buoyant, such that the issue of particles was solved by not agitating the solution after setting for at least 12hrs, then filling the pump from the bottom of the plastic bottle. When solutions passed through the rig was studied no contaminant particles were observed. The solutions seemed homogenous and repeatable, giving consistent viscosity results in the low shear regime.

As the NaCl and $CaCl_2$ concentration in the stock solution are known, the concentration in the prepared solutions can be calculated and the result is given in Table 5-1. In the calculation the density of all solutions are considered to be 1kg/L.

Table 5-1 Composition of polymer solutions

Polymer	Polymer conc	NaCl conc	$CaCl_2$ Conc
FLOPAAM 3630s	600ppm	23 g/L	0,825 g/L
FLOPAAM 3630s	1500ppm	21 g/L	0,33 g/L

5.2 Equipment

During the experimental runs the following equipment was used:

Pump:

Teledyne ISCO 500D syringe pump.
Flow rate 0.001-204 ml/min
Pressure range 0-258 bar

Pressure measurements:

Teledyne ISCO pressure transducer 0-258 bar
Kulite XTM 190-100G transducer 0-7bar
Vertical polycarbonate tube attached to pressure reservoir with a metering scale measuring "liquid column" 0-60mbar

Amplifier/DAQ:

HBM Quantum X MX410 connected via network cable
Catman Easy AP software

Tubing:

Swagelock 1/8" 0.035" wall thickness seamless 316SS tubing (1.397mm Inner Diameter (ID))

1/16" seamless SS tubing of unknown manufacture. ID approx. 300 micron

For the tubing the ID was "calibrated" with water through equation (4.20) as an accurate inner diameter is important for calculating apparent viscosity.

This was done as follows:

All tubes were run with distilled water at various flow rates in the laminar region, then the ID was adjusted until the calculated apparent viscosity from the Haagen Pouisulle equation (4.20) was 1cp. For the shortest capillary tube the pressure loss was not linear with flow rate, indicating some sort of vortex or turbulent inlet phenomena. For this pipe the pressure loss at the lowest flow rate was used to find the ID.

Most of the experimental runs where inside the pressure range of the Kulite transducer. The transducers were connected on the "filling" side of the pump so that they measured static pressure only, with no flow that can cause errors. The experimental setup can be seen in Figure 5-1

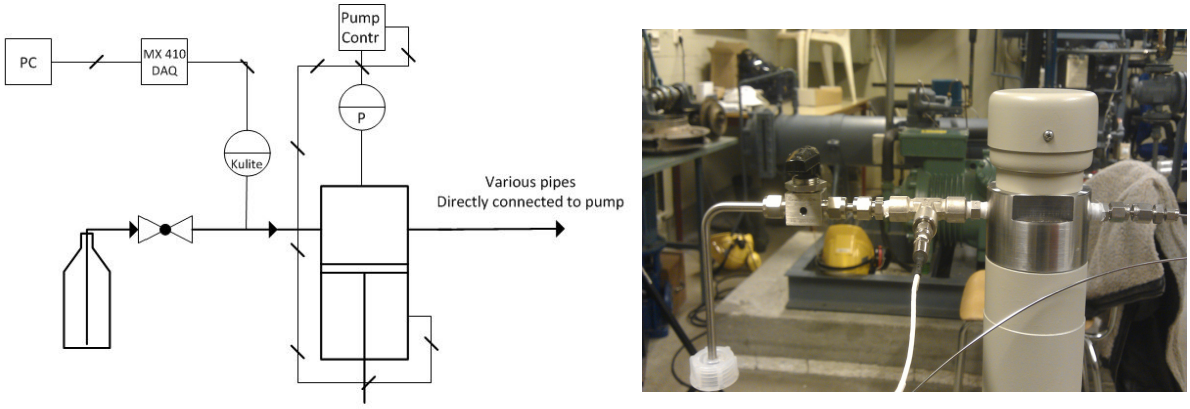

Figure 5-1 Experimental setup

Cutting capillary tubes with ID below 1mm can be challenging, and burring in the ends after cutting can significantly affect the pressure loss. When cutting the capillary tubes (300micron) the following procedure was used:

1. Tube was cut using a Dremel tool with a diamond cutting disc at high speed (35 000rpm)
2. Ends were deburred, first with a coarse metal file, and then finer and finer grit ending with 750 grit diamond knife-sharpener.
3. Inside was deburred using a syringe tip
4. Tube was flushed at high flow rate (10 m/s+ velocity) with water to remove any residue and burrs.

As the accuracy of the Kulite sensor was unknown, the sensor was checked for accuracy in both the normal operating range (2, 5 and 7bars) as well as in the range of 0-100mbar. The accuracy at 2,5 and 7 bars was controlled using a GE DPI 620 pressure calibrator. During this control the calibration data supplied by the sensor manufacturer fitted exactly with the pressure calibrator readings, so that the original calibration data from the manufacturer was used.

To control the accuracy of the Kulite sensor at low pressures the sensor was connected to the pump together with an U-tube manometer. Using the factory sensor calibration, multiple data points were recorded in the 0-100mbar range going from both zero pressure and 100mbar. The results of this control can be seen in Figure 5-2.

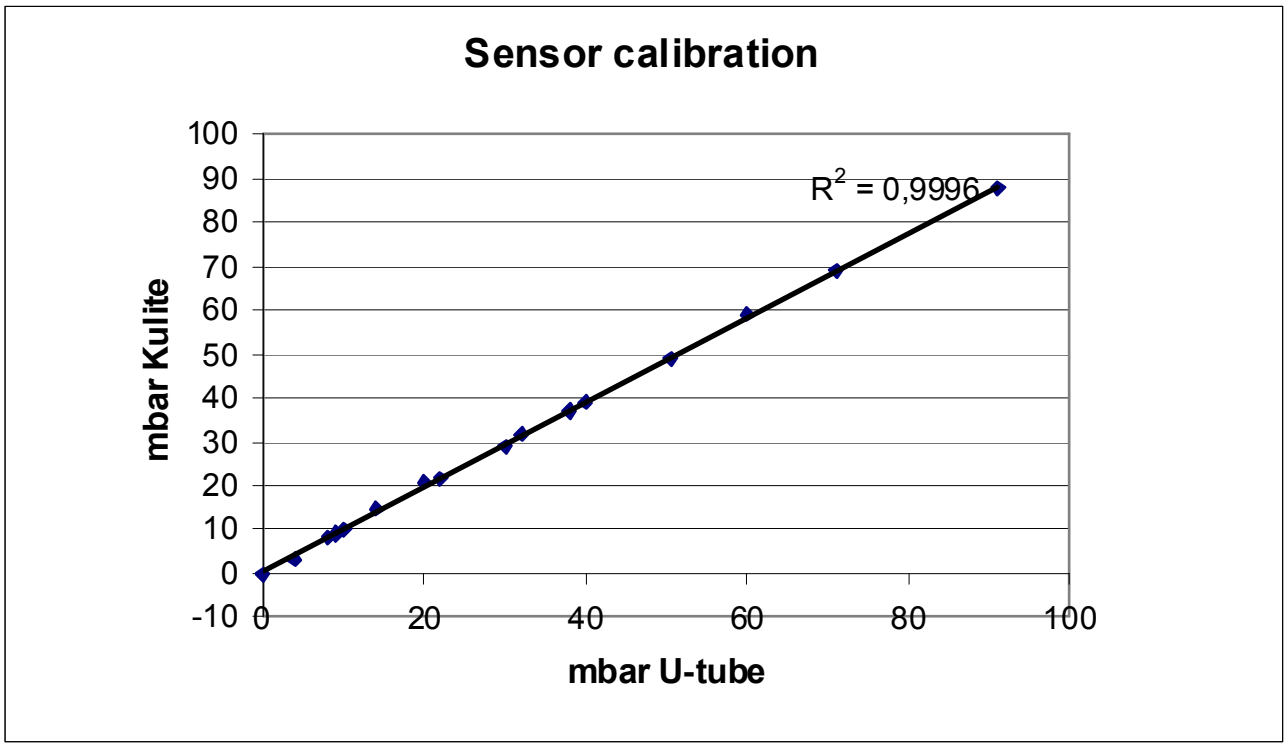

Figure 5-2 Kulite low pressure linearity, accuracy and calibration control

As seen in Figure 5-2 the Kulite sensor was both highly linear and accurate down to a close to zero pressure. The largest discrepancies observed was due to zero point drift (aprox 10-15mbar) when the sensor was left for 1hr+ without re-zeroing. This was solved during the experimental runs by relieving the pressure in the pump and controlling the zero point often.

5.3 Experimental procedure

The procedure during experiments was as follows:

1. If not already done for the particular pipe, multiple flow rates were recorded with water and the pipe ID was calibrated. If this was done earlier, then a selection of flow rates was ran with water to control the experimental rig. This “test” with water showed excellent agreement with previously recorded pressure loss data for water and was used as a control for all applicable tubes every time a new experimental series was started.

2. After calibrating ID or controlling the rig with water, the pump reservoir was completely emptied of water and filled with polymer. When filling a fill rate of 10ml/min through a ¼” filling tube was used to reduce risk of degradation.

3. The capillary tube was attached to the pump after filling, pressure transducer was zeroed and the recording of data started from low flow rate and upwards. Every fifth data point the zero point drift of the pressure transducer was checked. If a zero point drift was observed the sensor was re-zeroed and the recorded pressures at lower flow rates were double checked.

4. When reaching the end of the series the flow rates were reduced again, double checking the recorded pressures at 3-4 of the data points.

5. When switching from 600ppm to 1500ppm polymer the pump was not flushed with water, only completely emptied and then re-filled with higher concentration polymer.

6. At the end of the day/series the pump was filled up completely with water and then emptied twice to flush away any residual polymer solution. During this “cleaning” the tubes that had been used was also flushed with water.

5.4 Experimental results and discussion

The first experimental series conducted when settling on what tubes and polymer concentration to use was studying the shear thinning effect at low shear rates. The main motivation for this is that these data are readily available, so that it is a good control of the rig and methods used. After this the shear thinning viscosity at high shear rates was recorded using a long 300micron tube. Furthermore the inlet effects were studied at different shear

rates by using two short capillary tubes, one with a length/radius of approx 200 and one with (L/R) of approx 500. The results of the experimental series will be presented in the following subchapters. The original pressure/flow rate data can be found in appendix A. Table 5-2 summarize the dimensions of the tubes used, what "name" they are given in this chapter, as well as the "calibrated" diameter from running with water.

Table 5-2 Pipes and dimensions

Legend name in this chapter	Length (m)	Inner-Diameter adjusted with water (μm)	L/R (-)
1400 micron	0.35	1310	534
300 micron LR200	0.033	307	215
300 micron LR500	0.0755	325	465
300 micron LR INF	1.89	325	11631

The inner-diameters found when "calibrating" with water seem reasonable when considering that these tubes are not carefully calibrated capillary tubing with an exact ID, and that they are made for transporting fluids in an instrument, not for viscosity determination. The book in [4] recommends using the same approach as in this work to "calibrate" the diameter using a fluid of known viscosity as an accurate diameter is very important for viscosity calculations. (apparent in eq. (4.20)).

In all results the apparent viscosity is calculated from eq. (4.20), plotted against "Newtonian" wall shear rate from eq.(4.22). u_{avg} is defined in eq.(5.1) with Q being volume flow rate. The pressure is not corrected for kinetic energy effects and viscous heating is not considered as these effects should be negligible.

$$u_{avg} = \frac{\dot{Q}}{A} = \frac{\dot{Q}}{\pi r^2} \tag{5.1}$$

It can be argued that the "Newtonian wall shear-rate" defined in eq.(4.22) will not be entirely correct, especially for the shear thinning 1500ppm solution as shear thinning fluids will not have a parabolic velocity profile.

The actual shear rate at the wall can be calculated for shear thinning fluids using a correction determined by the fluids shear thinning properties. The choice of not doing this was motivated by the following four points: “Correcting” the wall shear rate for shear thinning requires accurate fluid properties or experimental runs in the same shear rate region using pipes with different diameters. The 600ppm solution is not especially shear thinning such that considering it Newtonian under shear is a reasonable assumption. The correction introduced is small. If eq.(5.2) [6] is used to calculate the wall shear rate with shear thinning, the difference between the shear rate compared to eq.(4.22) is approx 10% for the 1500ppm solution using shear thinning data from IRIS. Using a “Newtonian wall shear rate” is easily defined, can be easily be back-calculated to velocity and does not introduce any fluid dependent properties.

$$\left(\frac{1+3n}{4n}\right)\frac{4u_{avg}}{R} \tag{5.2}$$

5.4.1 Shear thinning

Figure 5-3 shows the calculated apparent viscosity of the two chosen concentrations of FLOPAAM 3630s, prepared as described previously and compared to measured viscosity of FP3630s at International Research Institute of Stavanger (IRIS). The data was recorded using the 1400 micron tube. The results from water at this tube are also plotted. Pressure was measured using a vertical tube at the inlet side, reading of liquid height and then calculating static head in the reservoir. The tube outlet was aligned at the same height as the reference point at the tube used for pressure estimation using a laser levelling device. This height was also confirmed at the end of the series by stopping the pump and checking that the level settled at the reference “zero” point. The results accuracy compared to those found at IRIS was found to be satisfactory. The largest discrepancy found was at the lowest flow rate of the 1500ppm solution. This may be due to the way pressure was measured, having a long “settling” time at low flow rates. It is also in the low range of what pressure can be measured using the said vertical tube, and thus has a lower accuracy at the lowest rates. At the highest shear rate measured at IRIS (500 1/s) the viscosity was found to increase. It is not known why this is the case, but it might be due to being at the high end of shear rates measureable with their device and thus this result is not included in the figure.

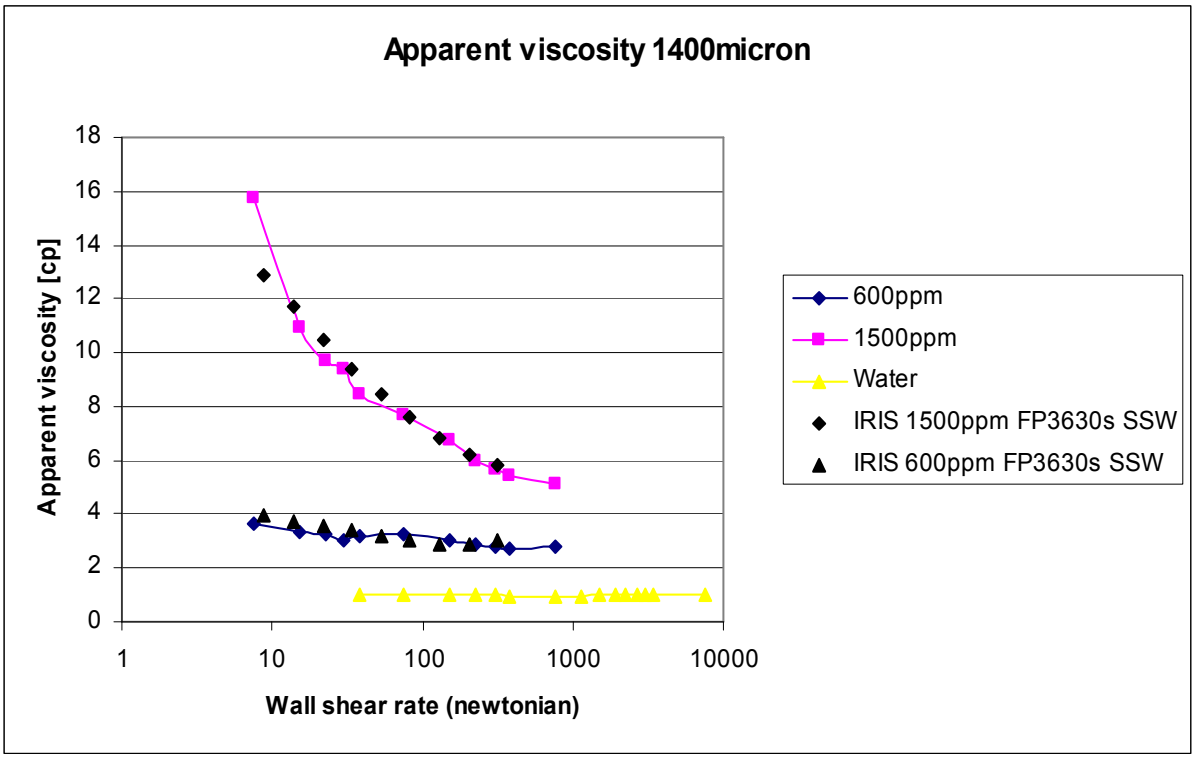

Figure 5-3 Apparent viscosity at low shear rate

The apparent viscosity at high shear rates has not been studied that much in literature, mainly because of limitations with the usual rotating viscometers commonly used for shear-viscosity characterization. Capillary viscometers show promise in measuring apparent viscosity at much higher shear rates, given that the flow is kept laminar. This can be achieved by reducing capillary diameter as the shear rate for a given Reynolds number is increased with a lower diameter. Figure 5-4 shows the shear thinning apparent viscosity at high shear rate for water and the two polymer concentrations calculated by using a long tube at 325 micron diameter (this is the diameter achieved from "calibration" with water).

The pressure was recorded with the Kulite

sensor.

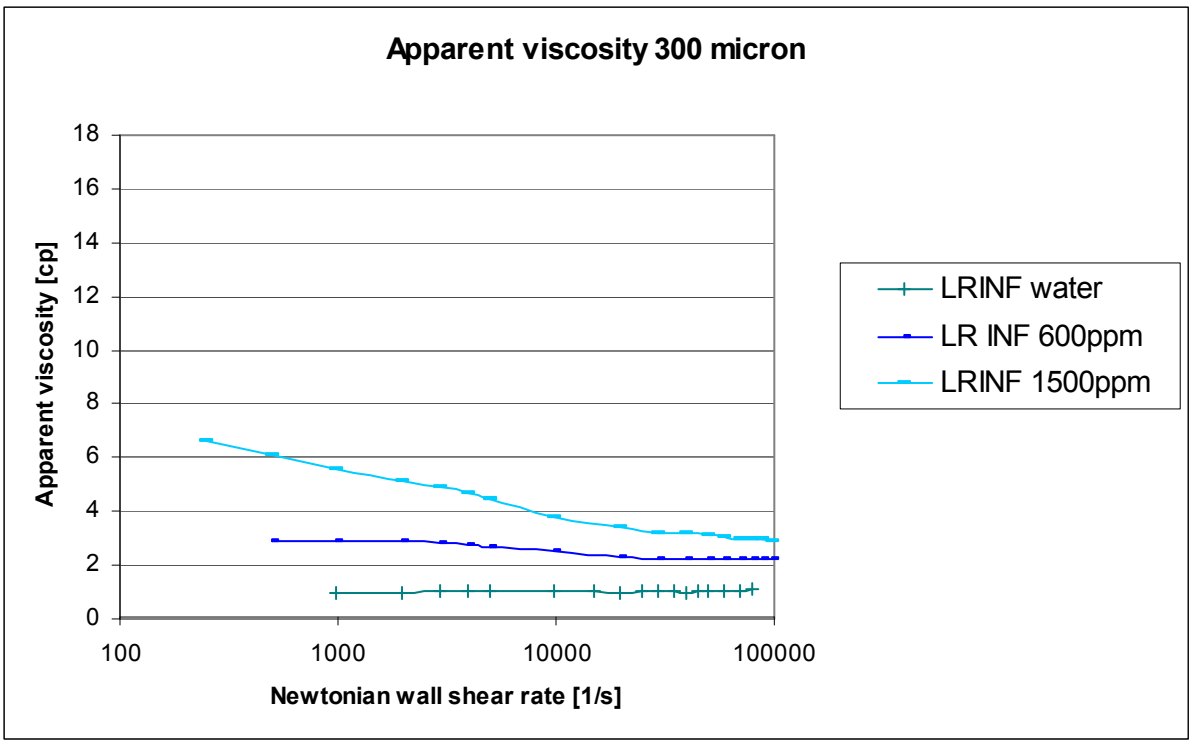

Figure 5-4 Apparent viscosity at high shear rate

Overall it was found that the rig are able to measure shear thinning- viscosity, and that the results seem reasonable compared to measurements at IRIS.

5.4.2 Increasing apparent viscosity

As it is hypothesised that the effect of "extensional viscosity" or "increasing apparent viscosity" found in porous media is a elongation effect, and that this effect should be visible in short capillary tubes, series with a L/R of both ~200 and ~500 was performed. Some increase in "apparent viscosity" was also observed for the 1400 micron tube used in the series given in Figure 5-3 but this effect was only observed at close to turbulent flow rates, so that these results are not included due to the uncertainties regarding flow regime.

Figure 5-5 shows the results recorded using the "short" 300 micron capillary tube at L/R ~200. It was found that for this tube the water pressure loss was not linear with flow rate, as can be seen from the increasing apparent viscosity recorded for water. This generally indicates that there might be turbulent flow or some turbulent or vortex inlet effect. It is worth noting that for the long 300 micron tube this was not noticed, so that if it is a turbulent phenomena it is likely limited only to the inlet section of the tube. As the pressure loss for water was not linear with flow rate the pressure loss at the lowest flow rate was used for "calibrating" the diameter of the tube. It was found that the apparent viscosity of the two

polymer solutions increased dramatically from the lowest flow rate and up to a local maximum before decreasing. This increase in apparent viscosity was not observed in the long capillary tube used in the series in Figure 5-4. As these tubes have more or less the same inlet geometry (and use the same fittings when attaching to the pump) the "inlet effect" observed in the short pipe likely occurs in the long pipe as well but is not observable due to the high pressure losses involved due to the pipe length.

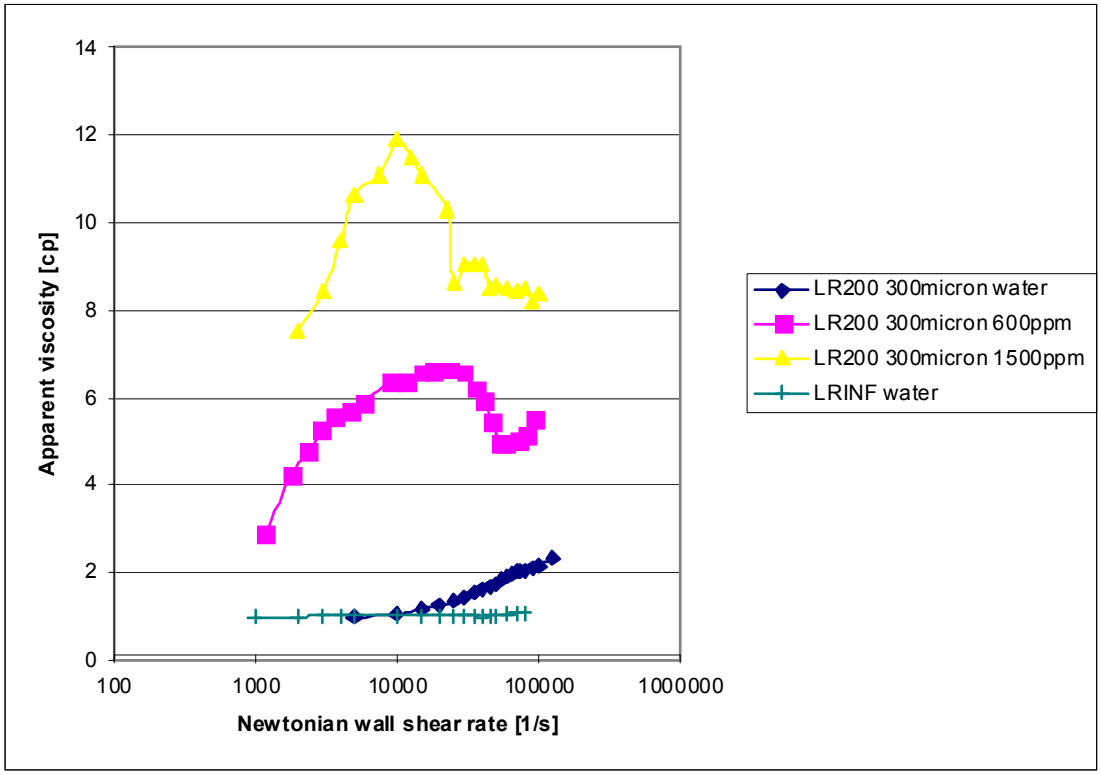

Figure 5-5 Increasing apparent viscosity LR200

Figure 5-6 shows the results recorded using the "medium" capillary tube at 300micron and L/R ~500. The results show an increasing apparent viscosity with flow rate, but not of the same magnitude as in the short pipe. This together with the fact that no increase was observed for the "long" tube further confirms that the observed increase is indeed some inlet effect. The results from the three lengths of 300 micron tubes can most easily be interpreted as a superposition of an inlet loss and pipe loss as given in eq.(5.3) where the last term is from the Haagen Poiusulle equation (4.20). From eq.(5.3) it can be shown that if the inlet loss is constant at one rate for the three pipes, the calculated apparent viscosity from the Haagen Pouisulle equation without considering inlet effects will be a function of pipe length, with the apparent viscosity approaching the shear viscosity for an infinite tube.

$$\Delta P = \Delta P_{inlet} + \Delta P_{pipe} = \Delta P_{inlet} + \frac{8u_{zavg}\mu L}{R^2} \qquad (5.3)$$

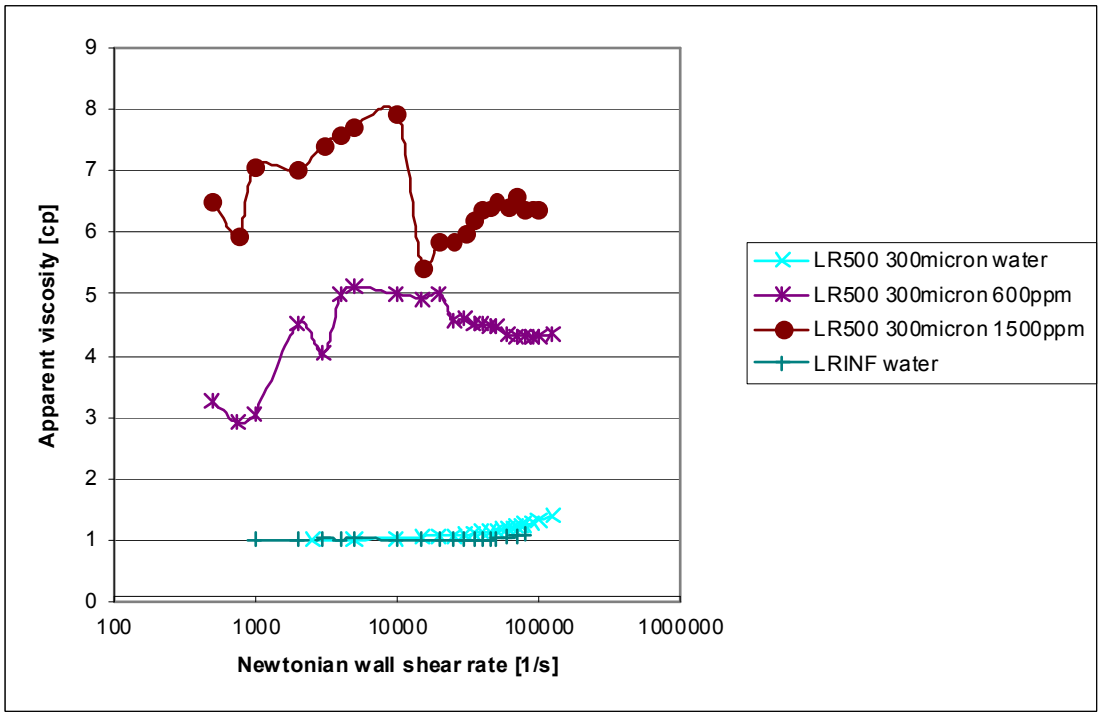

Figure 5-6 Increasing apparent viscosity LR500

Figure 5-7 and Figure 5-8 show the apparent viscosity from all experimental series plotted together for 600ppm and 1500ppm FP3630s respectively. The accuracy in the overlapping region for the different series seems reasonable when considering that this region is the region of the individual series that are likely to have the lowest accuracy due to low pressure loss for the 300 micron pipe. It was found that an increasing apparent viscosity with flow rate was observed for both the 600ppm and 1500ppm solutions in short capillary tubes with a local maximum and then decrease. As shown in eq. (5.3) if considering the increase a "point loss" inlet effect the magnitude of this local maximum should increase with shorter capillary tubes (lower L/R ratio) and the inlet effect should not be visible as an increase in the apparent viscosity if the pipe is sufficiently long so that the pipe loss is very large compared to the inlet loss. This was observed in the experimental series, so that it is reasonable to conclude that the observed increase in apparent viscosity is an inlet effect, and not an increase in shear viscosity at high shear rates. This result also fits well with the explanation of increasing apparent viscosity in porous media being due to a coil stretch transition effect with high extensional viscosity and losses in elongation flows.

It is worth noting that the results neither confirm or disprove this coil stretch transition theory, they only show that the increase is due to an inlet effect, but not what the actual phenomena is. It is not likely that the inlet effect is due to thixotropy, i.e. the time dependent dynamic effect of shear thinning as the effect was observed for the 600ppm solution with a local maximum far larger than the bulk steady shear viscosity at low shear rates (zero shear viscosity).

When running the series in the short pipes the pressure started oscillating a little into the increasing viscosity region (1000-2000 1/s) with the polymers, but not with water and not in the “long” 300 micron pipe with polymer. This indicate that the phenomena leading to the inlet loss is unstable. In the unstable region the average pressure was recorded.

Why the apparent viscosity suddenly decreases at a critical flow rate for both solutions are thought to be due to excessive stretching and thus mechanical degradation, a theory that was pursued further in the following subchapter. The decrease are thought not likely to be due to a “turbulent drag reduction” effect as the data from water indicates that the flow is laminar, at least for the L/R 500 tube and “long” tube.

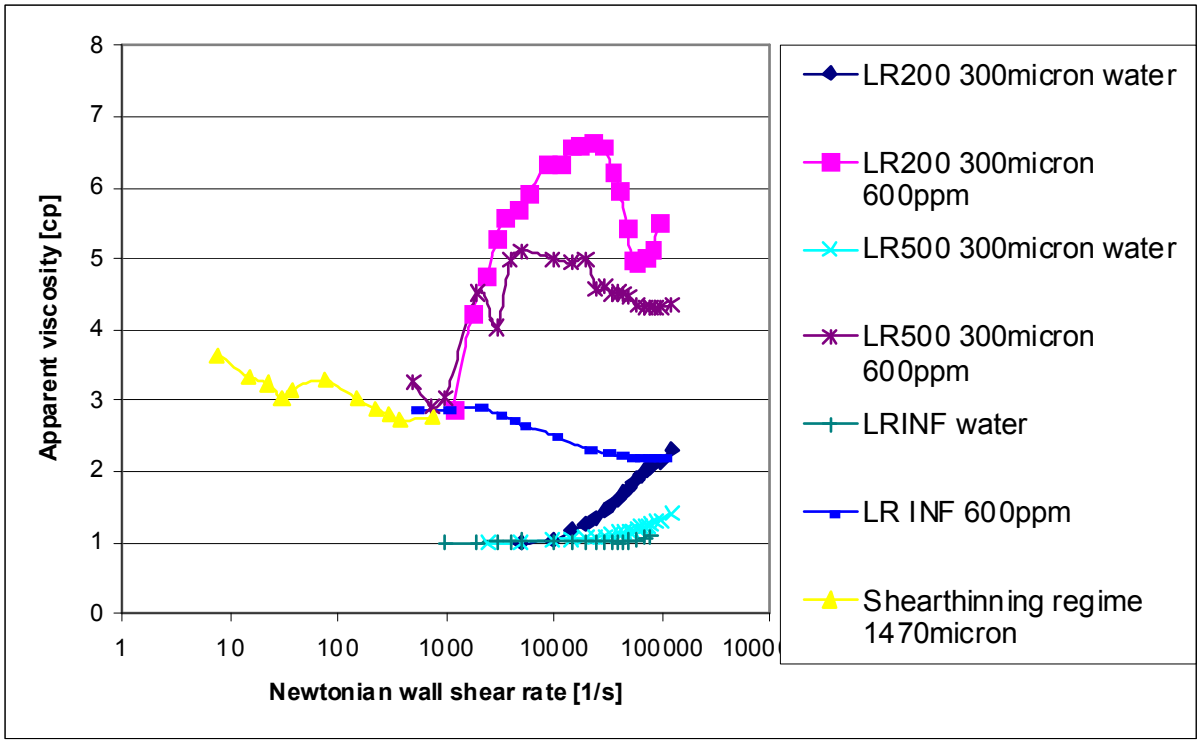

Figure 5-7 Apparent viscosity all experimental series 600ppm FP3630s

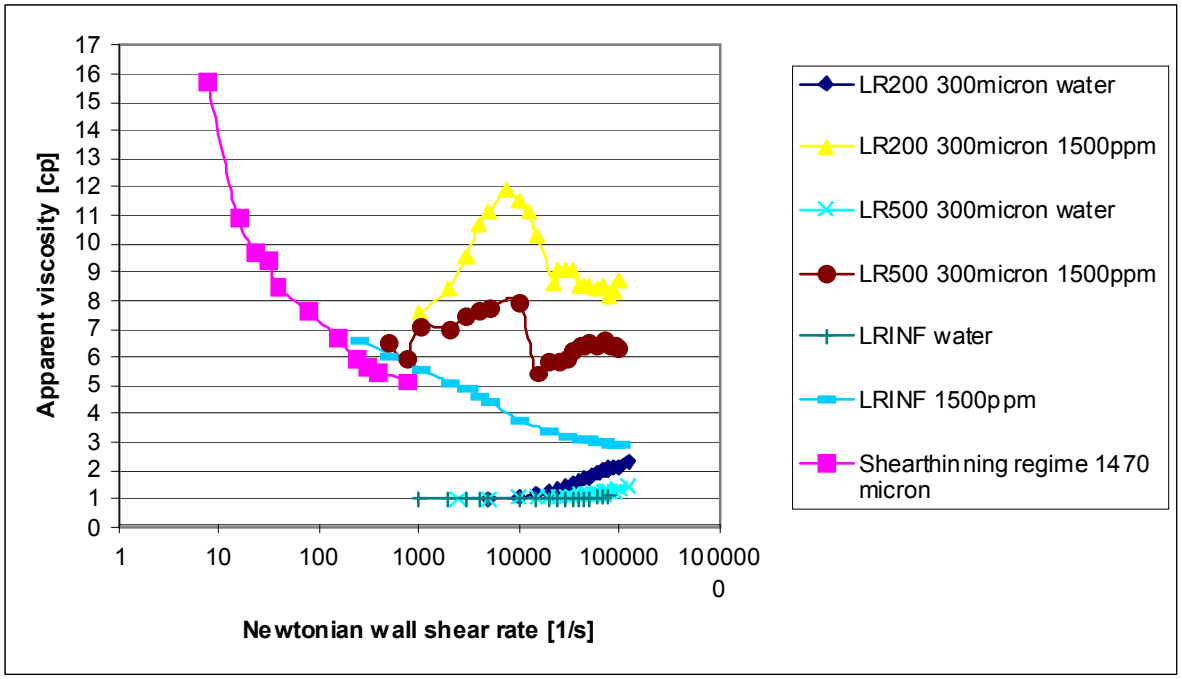

Figure 5-8 Apparent viscosity all experimental series 1500ppm FP3630s

5.4.3 Mechanical degradation

To study what happens at the local maximum and whether it is degradation causing the decrease in apparent viscosity after the local maximum, the following test was conducted:

600ppm FP3630s polymer solution was flowed through the rig at various flow rates and collected. The qualitative behaviour of the fluid after one pass at the various flow rates was then tested using a "ductless" siphon apparatus as described by J.G Southwick and C.W Manke [12]. The device used is compromised of a vacuum flask connected to suction and a tube. This tube is the dipped into the fluid and then raised out, forming a siphon effect of a measurable height and a critical height where the siphon cannot be sustained. This test should give a good qualitative measure of the fluids extensional properties. It is thought that if excessive extensional stress is the main route of degradation the scission of polymer chains and thus reduction of mean molecular weight has a dramatic effect on extensional properties [12]. No attempts to calculate the "extensional viscosity" from the ductless siphon was conducted, the siphon height where the siphon becomes unstable was only used as a quantitative "siphon height" describing polymer solution extensional properties.

Figure 5-9 shows the visually recorded ductless siphon height at the flow rates chosen after one pass through the rig in the LR200 300micron tube. It is stressed that the setup of the ductless siphon used in this work may have numerous sources for errors, human ones during reading of siphon height perhaps being the largest. Still the fluid show a clear and repeatable change in extensional properties over the local maximum. The magnitude of the different siphon heights are so large that it seems reasonable to conclude that the polymer does change extensional properties over the local maximum in apparent viscosity. This lends credence to the theory that mechanical degradation is likely at least part of the explanation for the decreasing apparent viscosity with flow rate after the local maximum. The change in siphon height occurred when passing a wall shear rate of approx 10 000 1/s. The work by A. Bhadwaj et al. [16] shows that a catastrophic filament failure occurs when using a FiSER extensional rheometer in the region of De =2-3, thought to be due to chain scission in the polymer solution. Predicting the Deborah number in the experimental geometry is very hard, but some work on predicting the ratio of inlet stretch to wall shear rate has been conducted using CFD in chapter 6.

The decrease in apparent viscosity appears to happen at a shear rate ~10 times that where the apparent viscosity increase. This ratio fits well with what is reported for porous media by

Stavland et.al. [3], where a decrease in effluent bulk viscosity due to degradation is found. If chain scission occurs at a De number of approx 3 as that reported by Bhadwaj et.al. [16] and stretch is considered proportional to shear then extensional effect starts appearing at a De number of 0.3 in the experimental geometry. This fits well with what Deborah numbers extensional effects are likely to become visible. (For instance the Oldroyd B model has a "infinite" extensional viscosity at De=0.5)

It is hard to conclude 100% what effect leads to the decrease in apparent viscosity over the maximum, but the results show that it is likely at least partly caused by mechanical degradation. The theory of the inlet effect causing high apparent viscosity and the decrease in apparent viscosity being due to excessive stretching and chain rupture in the inlet seem at least reasonable, with the ratio of strain rates where the extensional effects is observed and where the chain rupture occurs being supported by literature.

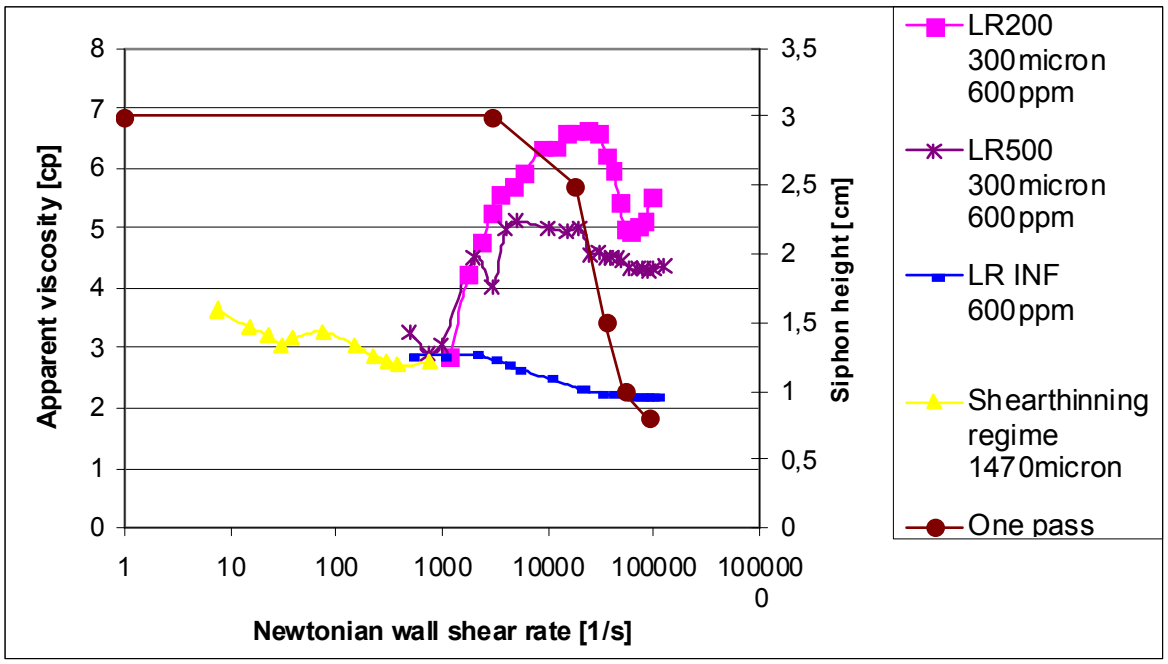

Figure 5-9 Ductless siphon height after one pass

6 Simulations

To further understand the experimental results and stresses in the experimental geometry, especially extensional strain rates CFD simulations was conducted on the experimental geometry. All simulations were performed in ANSYS Fluent 13 and all meshing was done in GAMBIT 2.4.6. As generalized Newtonian models are not able to predict viscoelastic phenomena no further work was done with this wrt. to simulations. To increase understanding of the viscoelastic flow, and to see if the models is able to replicate the increased inlet losses, a 2D Oldroyd-B viscoelastic model was implemented in Fluent using user defined functions. The viscoelastic Oldroyd-B model was not able to replicate the high inlet losses observed experimentally, but this is a well known problem for many viscoelastic models in CFD simulations. [22]

Some work on benchmark geometries was conducted to try to validate the implemented Oldroyd-B model but further work on benchmarking and stability is required.

A series of simulations were done to study the proportionality of the stretch rate in the inlet to wall shear rate for Newtonian fluids. This was done to study the validity of plotting results against wall shear rate and the often used assumption that wall shear rate and stretch rate is proportional.

6.1 Implementation of viscoelastic equations

The implemented Oldroyd-B model was derived via eq.(4.14) and (4.15). When writing eq. (4.15) out in 2D, using the definition of the upper convected derivative in eq. (4.12) eq. (6.1)-(6.6) is achieved.

$$\tau_{pij} + \lambda_1 \overset{\nabla}{\tau}_{pij} = \mu_p \dot{\gamma}_{ij} \tag{6.1}$$

$$\dot{\gamma} = \begin{bmatrix} \frac{\partial u}{\partial x} & \frac{1}{2}\left(\frac{\partial u}{\partial y} + \frac{\partial v}{\partial x}\right) \\ \frac{1}{2}\left(\frac{\partial u}{\partial y} + \frac{\partial v}{\partial x}\right) & \frac{\partial v}{\partial y} \end{bmatrix} \tag{6.2}$$

$$\overset{\nabla}{\tau}_{11} = \frac{\partial \tau_{11}}{\partial t} + u\frac{\partial \tau_{11}}{\partial x} + v\frac{\partial \tau_{11}}{\partial y} - 2\tau_{11}\frac{\partial u}{\partial x} - \tau_{21}\frac{\partial u}{\partial y} - \tau_{12}\frac{\partial u}{\partial y} \tag{6.3}$$

$$\overset{\nabla}{\tau}_{12} = \frac{\partial \tau_{12}}{\partial t} + u\frac{\partial \tau_{12}}{\partial x} + v\frac{\partial \tau_{12}}{\partial y} - \tau_{12}\frac{\partial u}{\partial x} - \tau_{22}\frac{\partial u}{\partial y} - \tau_{11}\frac{\partial v}{\partial x} - \tau_{12}\frac{\partial v}{\partial y} \tag{6.4}$$

$$\overset{\nabla}{\tau}_{21} = \frac{\partial \tau_{21}}{\partial t} + u\frac{\partial \tau_{21}}{\partial x} + v\frac{\partial \tau_{21}}{\partial y} - \tau_{11}\frac{\partial v}{\partial x} - \tau_{21}\frac{\partial v}{\partial y} - \tau_{21}\frac{\partial u}{\partial x} - \tau_{22}\frac{\partial u}{\partial y} \tag{6.5}$$

$$\overset{\nabla}{\tau}_{22} = \frac{\partial \tau_{22}}{\partial t} + u\frac{\partial \tau_{22}}{\partial x} + v\frac{\partial \tau_{22}}{\partial y} - 2\tau_{22}\frac{\partial v}{\partial y} - \tau_{12}\frac{\partial v}{\partial x} - \tau_{21}\frac{\partial v}{\partial x} \tag{6.6}$$

Combining the equations above give eq (6.7) written in Einstein notation for compactness. If (6.7) are to be implemented in a CFD package the four stress components τ_{11} τ_{12} τ_{21} and τ_{22} has to be transported scalars with their own PDE's being solved.

$$\frac{\partial \tau_{ij}}{\partial t} + v_k\frac{\partial \tau_{ij}}{x_k} = \tau_{kj}\frac{\partial v_i}{\partial x_k} + \tau_{ik}\frac{\partial v_j}{\partial x_k} + \frac{\mu_p}{\lambda_1}\dot{\gamma}_{ij} - \frac{1}{\lambda_1}\tau_{ij} \tag{6.7}$$

The term $v_k\frac{\partial \tau_{ij}}{x_k}$ is solved in Fluent for convected user defined scalars [26], and the $\tau_{kj}\frac{\partial v_i}{\partial x_k} + \tau_{ik}\frac{\partial v_j}{\partial x_k}$ terms introduced through the upper convected derivate can be added as sources for the UDS together with the "real" source and sink $\frac{\mu_p}{\lambda_1}\dot{\gamma}_{ij} - \frac{1}{\lambda_1}\tau_{ij}$.

By default any UDS defined in Fluent without diffusion is solved as in eq (6.8) where S_φ is the sources defined by the user. [25]

$$\frac{\partial \rho\varphi}{\partial t} + v_k\rho\frac{\partial \varphi}{x_k} = S_\varphi \tag{6.8}$$

Thus the sources defined in Fluent for the four polymer stress components is as given in eq. (6.9).

$$S_{\tau_{ij}} = \rho(\tau_{kj}\frac{\partial v_i}{\partial x_k} + \tau_{ik}\frac{\partial v_j}{\partial x_k} + \frac{\mu_p}{\lambda_1}\dot{\gamma}_{ij} - \frac{1}{\lambda_1}\tau_{ij}) \tag{6.9}$$

6.1.1 Implementation in Fluent

To implement the Oldroyd-B model in Fluent a combination of user defined scalars (UDS) and momentum sources was used. It can be shown in eq. (6.3)-(6.6) that the stresses for the Oldroyd-B model is symmetric over the diagonal, that is $\tau_{ij} = \tau_{ji}$, such that only three stresses has to be transported. As the computational load does not increase that much with 3 as compared to 4 UDS's this approach was not used and all four stresses were implemented in the model. The full C library written and used is given in Appendix B.

The sources implemented for each of the four scalars was as given in eq.(6.9).

Eq.(6.1) coupled with the momentum equations was done as follows:
All cases were solved as laminar flow, with a solvent viscosity defined in Fluent. The extra polymeric stresses (UDS's) were then solved and introduced into the momentum equations as momentum sources. To enhance stability "clipped" derivatives was used in the UDS sources, in Fluent named Reconstructed Gradients (RG). As RG data are normally deleted to free solver memory before the UDS transport equations are solved the following has to be set in Fluent:

solve>set>expert Keep temporary solver memory from being freed? (y)

The C library is written in Visual Studio 2013 and has to be compiled in Fluent. For the Fluent compiler to work Fluent has to be opened trough the VS2013 x64 Cross Tools Command Prompt. Before compiling the C library four user defined scalars should be added to Fluent through Define->User-Defined->Scalars and convective transport should be solved through "mass flow rate". Then the diffusion constants for each UDS should be set to zero in the material properties tab and all the sources added through the Cell-Zone-Conditions tab with "Sources" checked.

6.1.2 Solution Procedure

Due to the intricate coupling of the nonlinear Navier Stokes equations generally a Pressure Velocity-coupling algorithm has to be utilized during the solving of equations. Fluent has multiple coupling algorithms, with their own strengths and weaknesses.

When solving the Oldroyd-B model the SIMPLE (Semi Implicit Method for Pressure Linked Equations) was used. A general overview of the SIMPLE algorithm can be seen in Figure 6-1.

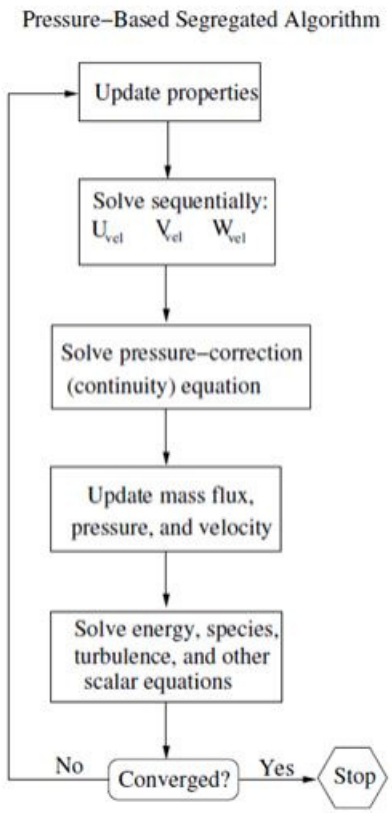

Figure 6-1 Pressure velocity coupling algorithm[27]

In Fluent the implemented Oldroyd-B model is solved as follows:
At the first iteration the flow field is solved using the "solvent viscosity" only. At the end of the loop reconstructed velocity gradients (RG) are used to solve the four stress components introduced through the Oldroyd model as user defined scalars, with the nonlinearity introduced through the upper convected derivative as a source term as in eq.(6.9). For the next iteration (and following iterations) the momentum equations (first step) is solved with momentum sources. These sources are based on the transported stresses so that the momentum source for x-momentum is eq.(6.10) and y momentum eq.(6.11)

$$S_{Mx} = \frac{\partial \tau_{11}}{\partial x} + \frac{\partial \tau_{12}}{\partial y} \tag{6.10}$$

$$S_{My} = \frac{\partial \tau_{21}}{\partial x} + \frac{\partial \tau_{22}}{\partial y} \tag{6.11}$$

6.2 Validation of Oldroyd-B model

Simulations on documented benchmark geometries were run with the implemented Oldroyd-B model for validation, namely the vortex shedding behind cylinder [19], cross slot flow bifurcation [20], 4:1 contraction [21] as well as a test of the model under simple shear. The test was run to mainly get a view on the qualitative behaviour of the implemented model. The model was not able to produce the pressure drop in inlet geometries observed experimentally. This is a well known problem with viscoelastic constitutive equations. As thorough benchmarking of implemented models is very time consuming, requiring different meshes and discretization schemes trials as well as different geometries this was not done in this work due to time limitations. Viscoelastic constitutive equations have been shown to be very discretization and mesh dependent due to numerical diffusion (in equations not having a diffusion term.) The simulations presented below are all run with the SIMPLE algorithm, second order upwind momentum discretization, and first order upwind discretization for the "extra stresses". Using a first order scheme for the extra stresses introduced in the model has been shown [19] to be overly diffusive as the equations has no "natural" diffusion, but it does make convergence easier. In all cases the simulations were run in transient and the polymer time constant was increased incrementally each simulation until the simulations start diverging. For all simulations the residual convergence criteria was 10^-4 for all PDE's (x-momentum, y momentum, continuity and the four stress components).

It was found that the model under simple shear exhibit the behaviour predicted by simple solutions of the Oldroyd-B model, that is Newtonian behaviour with a viscosity being the sum of polymer and solvent viscosities. In other words the Oldroyd-B model yield the same pressure losses as a purely Newtonian simulation with a viscosity being $\eta = \eta_s + \eta_p$ under simple shear.

For the 4:1 contraction geometry the model show (at least qualitatively) the same behaviour as documented in other work. Many of the benchmark simulations on contraction flow have a very large polymer viscosity compared to solvent viscosity (much more than 10 times solvent viscosity). At this high polymer viscosities the model show very large convergence issues and divergence, something that appears to be (partly) helped by running smaller time steps/ higher under-relaxation. This is likely due to the "splitting" of polymer and solvent stresses, with the polymer stresses lagging one iteration behind. Figure 6-2 shows contours of x-direction normal stress from the implemented Oldroyd-B model in a 4:1 contraction geometry.

The qualitative appearance of normal stresses in the elongational-flow region of the inlet and the normal stresses under shear (not appearing in Newtonian fluids) are in agreement with literature.

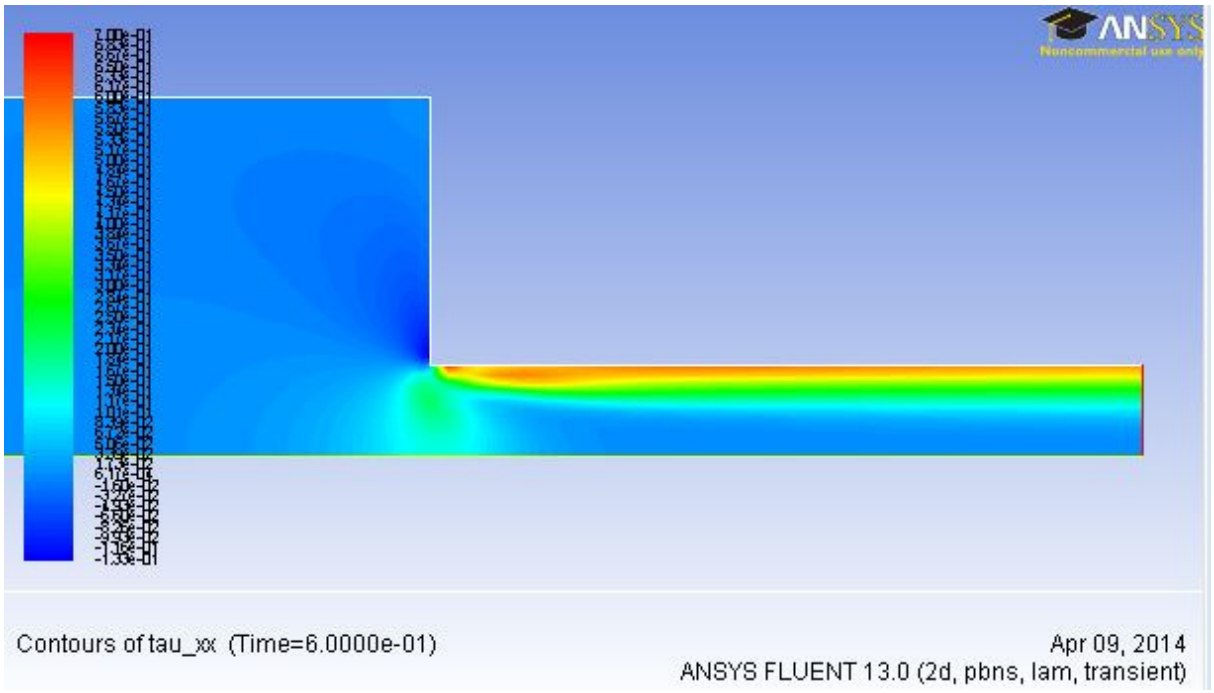

Figure 6-2 Contours of normal stresses in the x direction τ_{11} for a 4:1 symmetric contraction geometry

For the cross slot flow bifurcation the asymmetric bifurcation effect described in both literature, and only appearing for viscoelastic fluids was not observed. The appearance of "high" normal stresses at the stagnation point at low Deborah numbers match those of Rocha et al[20], but the simulations diverge at higher Deborah numbers (higher λ_1 time constant) before the asymmetric instability presents itself. Figure 6-3 shows the contours of y direction normal stress at the stagnation point in the cross slot flow geometry.

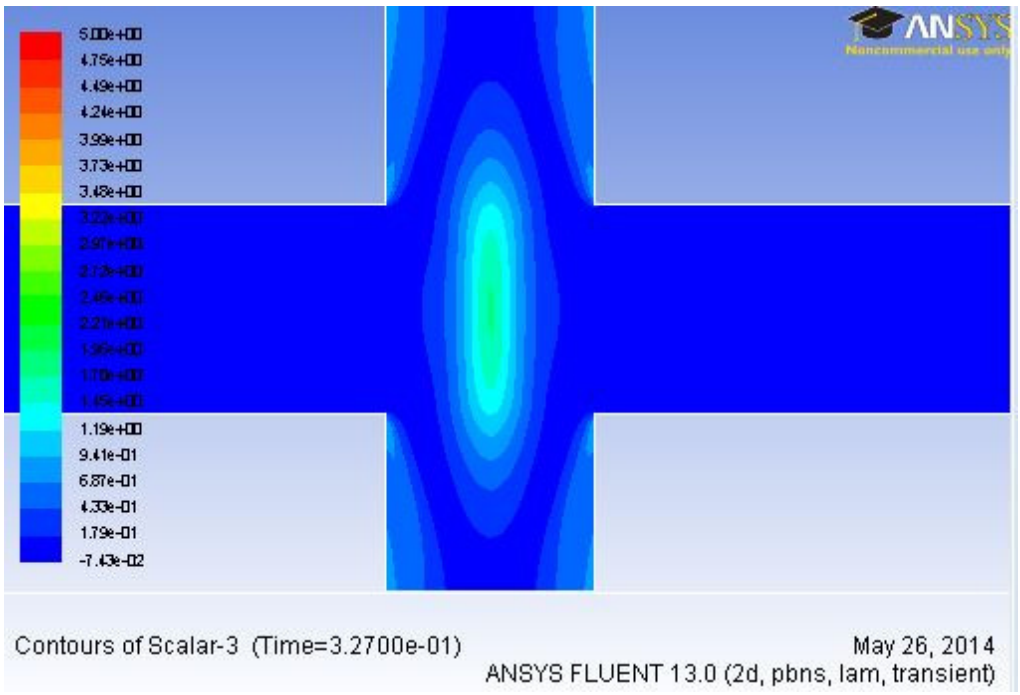

Figure 6-3 Contours of y direction normal stress τ_{22}

To study the models influence on vortex effects, vortex shedding behind a cylinder at Re=100 was studied with Newtonian fluids and the implemented Oldroyd-B model to study shedding frequency as literature show that viscoelasticity should reduce frequency. Lift coefficient and drag coefficient using default Fluent unit scaling was recorded in transient simulations such that frequency can be compared for the two simulations. The work by Oliveira [19] shows both a reduction in lift and drag on the cylinder, as well as a reduced frequency. This reduction of lift and drag was not observed in this work (actually a slight increase was observed) but the viscoelastic model reduces the shedding frequency as compared to Newtonian flow. This simulation did not use the same ratio of solvent/polymer viscosity as that by Oliveira, something that may explain why this reduction in lift and drag was not observed. Figure 6-4 shows the lift on the cylinder, and the different vortex shedding frequency in viscoelastic simulations as compared to the Newtonian simulations. As with all other benchmarking geometries the same issue with divergence when increasing the polymer time constant further was observed. This increase in time constant and thus Deborah number should according to [19] reduce the frequency further.

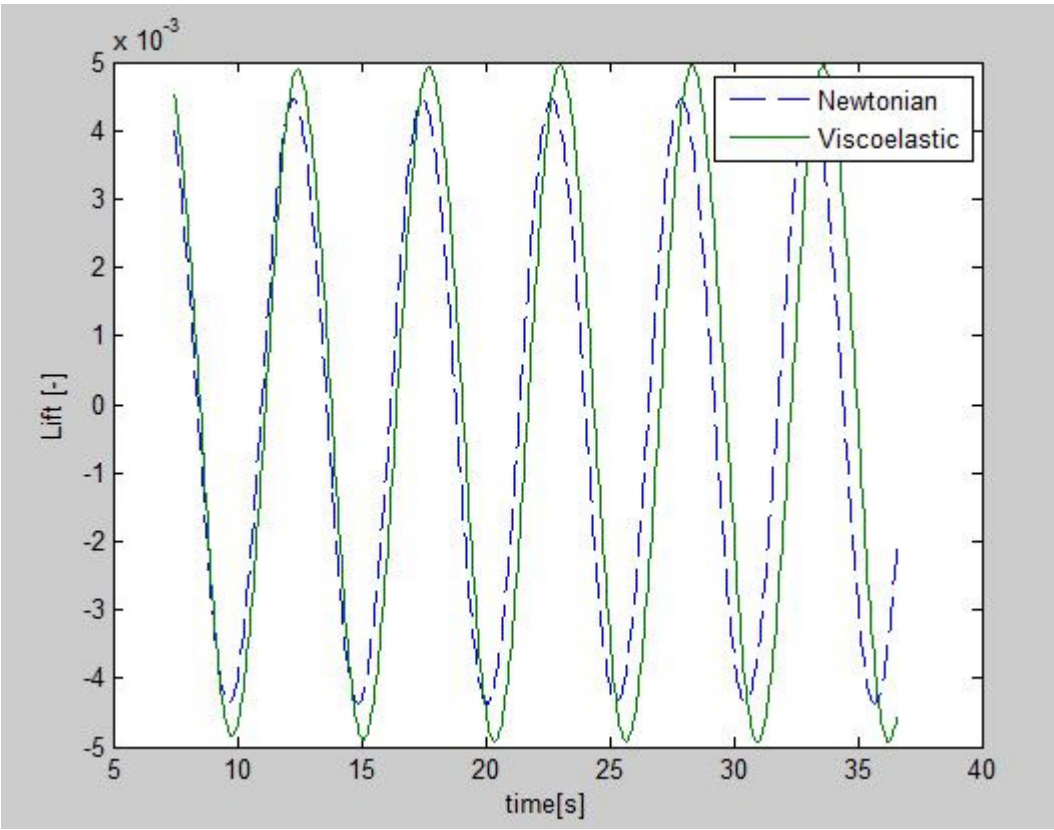

Figure 6-4 Vortex shedding with Newtonian vs. viscoelastic model

Overall the implemented Oldroyd-B model shows promise, but requires a lot more thorough benchmarking. The problem with divergence at higher De numbers is very likely at least in part a effect from the model itself, with the Oldroyd model having an infinite extensional viscosity at finite stretch rates. The implemented model does not help in explaining the "extensional" inlet effects with high inlet pressure losses observed experimentally in this work and thought being the same as that observed in porous media by others. This is a well known and documented issue with numerical viscoelastic models [22].

Most of the studies being used as test cases here have been done with FENE type models that does not have an unbounded extensional viscosity. That may in part explain why some of the phenomena observed could not be reproduced here as the FENE models are more stable due to the fact that they have a finite extensional viscosity.

6.3 CFD Simulation results and discussion

To study the deformation rates in the experimental geometry, and whether the stretch rate is proportional to wall shear rate, Newtonian simulations at different flow rates and viscosities were performed. Even though the capillary pipe used experimentally was connected to the pump with fittings, only the entrance to the capillary itself was simulated as the contraction ratio here is very dramatic compared to the fittings connecting the capillary to the pump.

Two inlet geometries was simulated to see the effect of geometry on the proportionality between stretch rate and wall shear rate.

The actual stretch rate compared to wall shear rate in the experimental geometry with polymers are likely not the same as for Newtonian simulations. Viscoelastic fluids have a tendency to enhance corner-vortex effects, and can cause quite dramatic asymmetric elastic instabilities in these type of contraction geometries [19]. Still the Newtonian simulations can give an indication on the geometry and velocity dependence of the proportionality between max shear rate and max stretch rate.

6.3.1 Meshes

The two inlet geometries studied can be seen in Figure 6-5 and Figure 6-6, from here on named “Inlet1” and “Inlet2”. Inlet1 is a sharp corner inlet, whereas Inlet2 has trapezoidal corners. Both geometries has roughly the same dimensions as the inlet in the capillary used experimentally with a contraction from 1/16” to 325micron inner diameter. Only half the geometry was simulated and the simulations run as 2D axisymmetric.

Both geometries was meshed with quadrilateral uniform elements of 0.005mm, and meshes had a element count of ~270 000.

The inlet was defined as a fully developed laminar velocity-inlet as in eq. (6.12) and implemented through a user defined function.

$$u(r) = 2u_{avg}\left(1 - \left(\frac{r}{R}\right)^2\right) \tag{6.12}$$

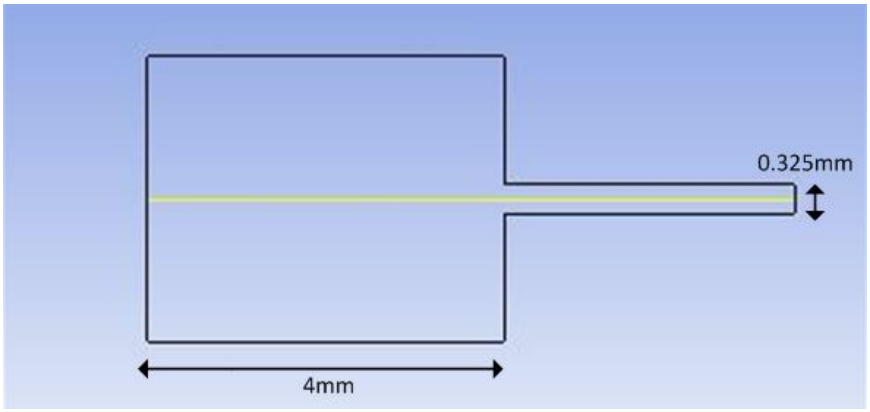

Figure 6-5 ”Inlet1” Geometry

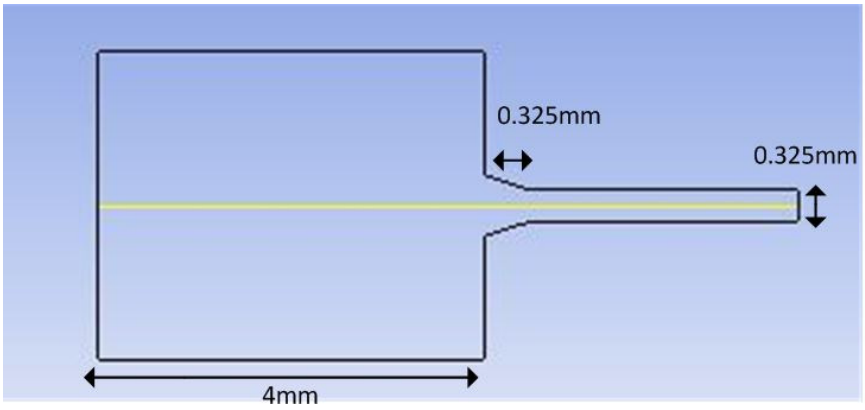

Figure 6-6 "Inlet2" Geometry

6.3.2 Convergence criteria

For all simulations the residual convergence criteria was set to 5*10^-4 for all equations and the vertex maximum stretch rate $\frac{du}{dx}$ was monitored at the centreline axis to judge convergence.

Coarser meshes were tried to check mesh independence and coarse meshes yielded results close to that of the “fine” meshes when using high order discretization schemes (Quick).

The fine meshes used for the simulations presented here were more or less independent on scheme (less than 1% change in max stretch rate when switching from first order upwind to second order upwind).

6.3.3 Results

Figure 6-7 shows the contours of velocity magnitude, strain rate magnitude and stretch ($\frac{du}{dx}$) for the Inlet1 geometry. The centre figure is the strain rate magnitude used to calculate "thinning" in generalized Newtonian models in Fluent, and it is thus obvious that for instance the Carreu Yasuda model will actually have thinning effects in the "stretch flow" inlet section where the extensional effects are believed to occur. For comparison the Oldroyd-B model in Figure 6-2 shows an "extra" normal stress in this region. The right hand figure shows the stretch rate only, with a high stretch rate where extensional effects are believed to occur in the experimental geometry.

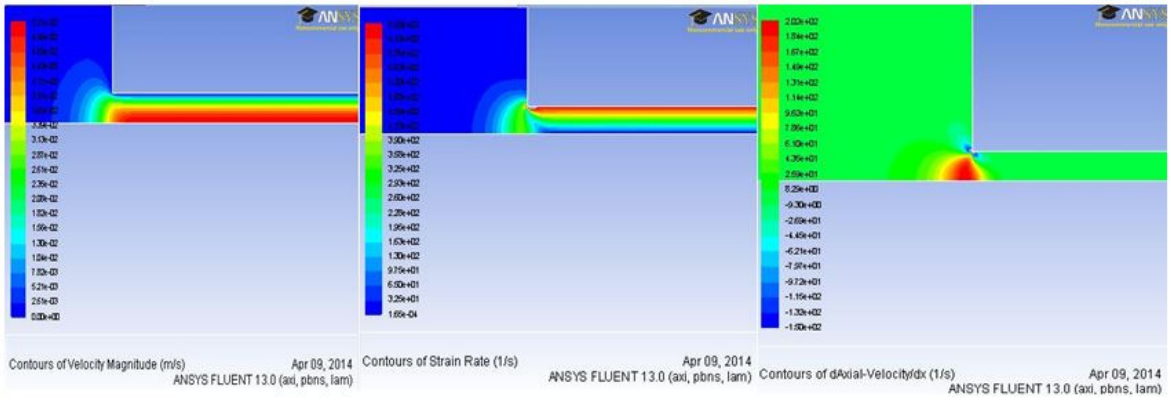

Figure 6-7 Velocity magnitude [m/s], strain rate magnitude [1/s] and stretch rate [1/s] in Inlet 1

To study the proportionality between stretch rate and wall shear rate and its velocity dependence (or independence?) a range of velocities covering wall shear rates from close to zero to 65000 1/s i.e. the same range as the experiments was simulated. To see the effect of geometry on the dependence both "Inlet1" and "Inlet2" were simulated using the same flow rates.

Figure 6-8 and Figure 6-9 show the result of said simulations and plotted using MATLAB. It is found that the proportionality between centreline max stretch rate and wall shear rate is not constant with velocity, but appears to approach a constant value. Comparing the proportionality in the two figures it is obvious that geometry is a very important factor. The exact inlet geometry of the experimental rig is hard to determine due to its small scale, but is likely somewhere in between Inlet 1 and Inlet 2 due to deburring.

The wall shear rate in the capillary section was found to be in excellent agreement with eq.(4.22).

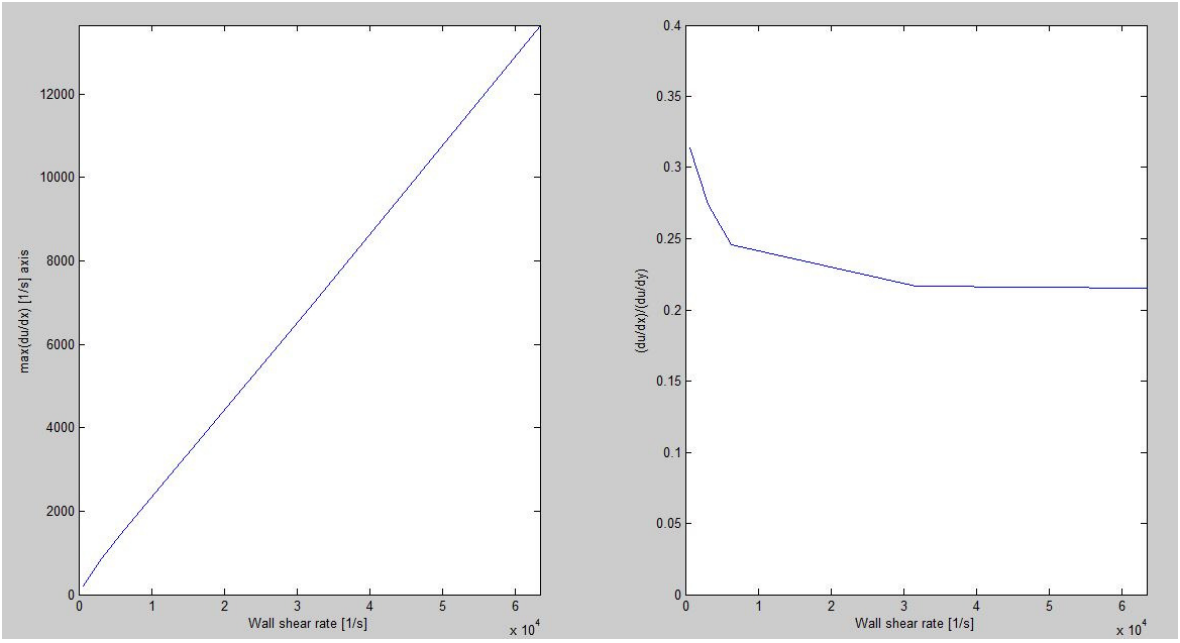

Figure 6-8 Max stretch rate at the centreline axis (du/dx) vs. max shear rate and proportionality (max du/dx)/max(du/dr) vs. shear rate for the Inlet 1 geometry

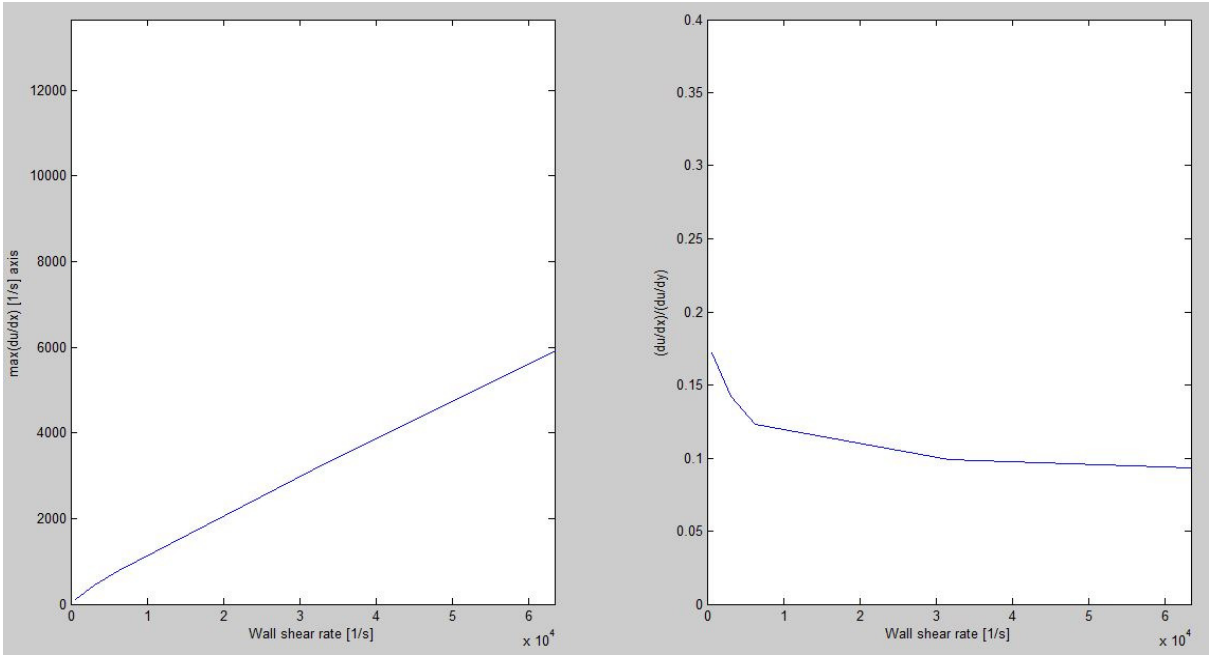

Figure 6-9 Max stretch rate at the centerline axis (du/dx) vs. max shear rate and proportionality (max du/dx)/max(du/dr) vs. shear rate for the Inlet 2 geometry

To study the effect of viscosity on the proportionality between centreline maximum stretch rate and wall shear rate, multiple simulations with different viscosity was conducted. For all the simulations the same flow rate was used. Figure 6-10 shows centreline max stretch rate at a wall shear rate of 6.33*10^3 for viscosities from 1-8 cp. That specific flow rate was chosen as it is in the region where the proportionality was found to be velocity dependent (not constant). The results show that for the given flow rate the maximum centreline stretch rate increases with viscosity. When considering that increasing the viscosity for a given rate is effectively reducing the Reynolds number the results in Figure 6-10 are showing the same trend as those in Figure 6-8 and Figure 6-9 that is the proportionality decreasing with increasing Reynolds number.

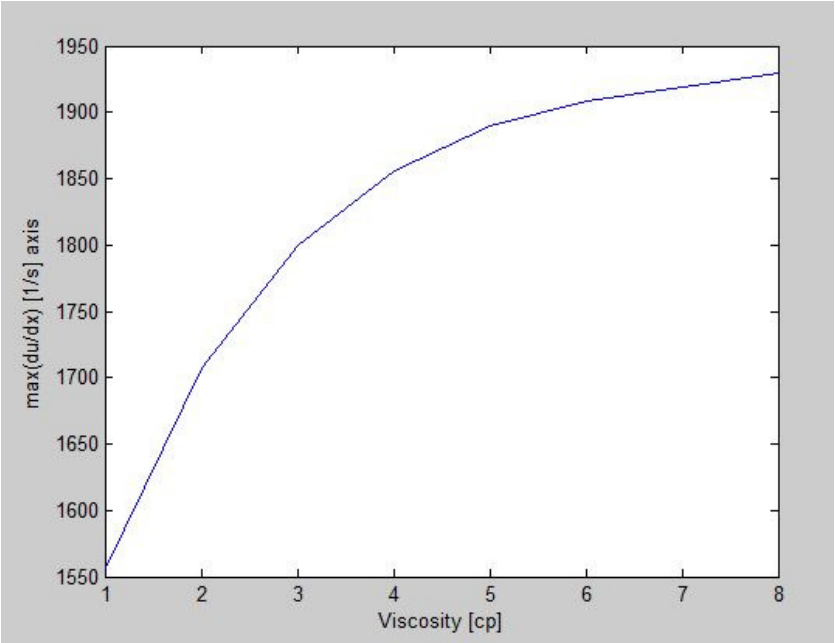

Figure 6-10 Effect of viscosity on maximum centreline stretch rate

One issue that is still to be addressed is whether the flow really can be described by "one" stretch rate for a complex flow geometry. The simplicity of considering only one maximum stretch rate is obvious, but as seen in Figure 6-11 the fluid actually passes through "all" stretch rates from zero to the maximum, and some of the fluid does not experience the maximum stretch rate at the axis. If stretch rates from CFD simulations are to be used to assess polymer time constants and thus De numbers (even semi quantitatively) understanding of the exact phenomena occurring in the inlet section for elastic polymers are required. This effect is not yet fully understood [22].

The effect of having high De polymer flows as opposed to Newtonian fluids in the inlet section on stretch rates is hard to quantify due to breakdown of numerical simulations, but other work with both simulations and experimentally show that the effect can be significant [17, 21, 22].

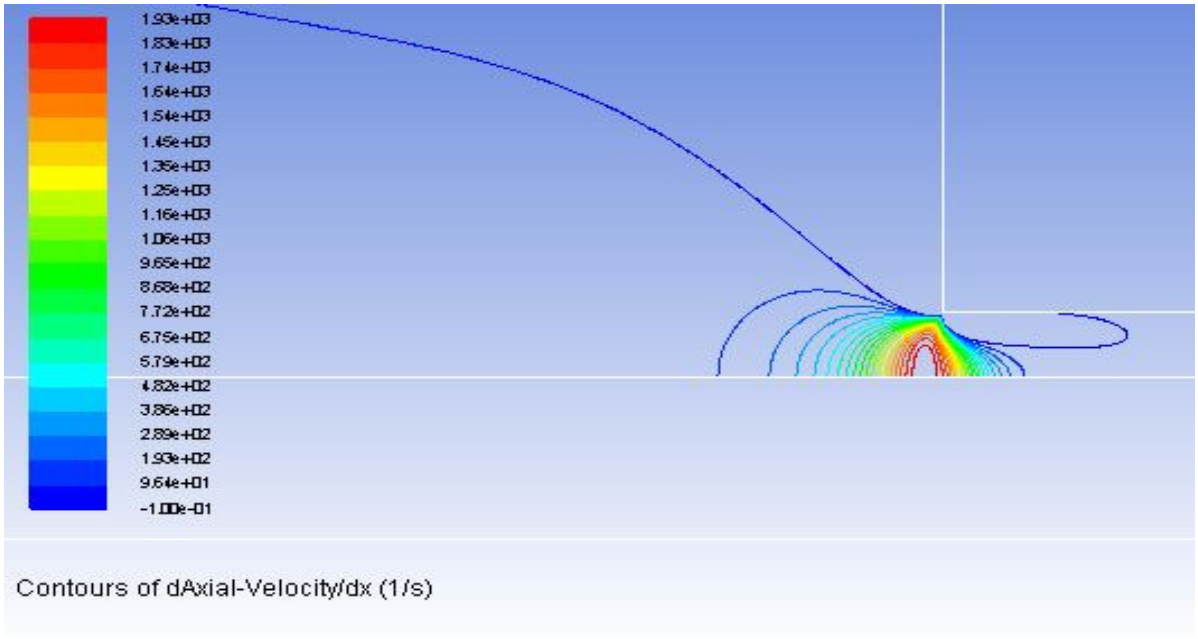

Figure 6-11 Contours of stretch rate Inlet 1

7 Conclusion

Through the experimental series it was demonstrated that a high inlet loss pressure loss was observed with HPAAM, found as a increase in apparent viscosity from the Haagen Pouisulle equation. At a critical wall shear rate the apparent viscosity for flow in short capillary tubes increase dramatically before reaching a maximum and then decreasing with flow rate. For both 600ppm and 1500ppm FLOPAAM 3630s this “thickening” effect starts to occur at a wall shear rate of approx ~1000 1/s for the capillary tubes used in this work. This result fits well with experimental data for HPAAM flow in similar geometries in literature. The apparent viscosity was found to have a local maximum and then decrease with flow rate. The decrease in apparent viscosity starts at approx 10 0001/s, or roughly 10 times the wall shear rate where the increase starts. This ratio fits well with experimental data from literature for flow of HPAAM in porous media. The “shear” rate where the increase in apparent viscosity is observed in porous media in literature is close to a order of magnitude lower then what found in the experimental geometry. This can have numerous explanations; The accuracy of the models used to calculate the shear rate in porous media is uncertain, also the fluids “history” may have a large impact on what stretch rate the extensional effects occurs

It was found that in the shear thinning regime viscosity determination from capillary tubes and pressure data is possible, and results have reasonable accuracy when compared to other rheometric devices such as cone and plate rheometers.

It is shown through the experimental series on different tube lengths that the increase in apparent viscosity is an inlet effect, not “shear thickening”, and it is thought that this effect is the same as that observed in porous media, caused by stretching of molecules in the stretch flow just at the inlet of the capillary. Oscillating pressure measurements in this flow range indicate that the inlet phenomena is unstable.

The decrease in apparent viscosity with flow rate after the maximum is thought to be due to mechanical degradation and chain “scission”. This theory is also partly validated from experimental data from a ductless siphon aperture, showing a decrease in the extensional properties of the effluent over the maximum in apparent viscosity.

An Oldroyd-B viscoelastic model was implemented through user defined functions and scalars in ANSYS Fluent to try to explain the inlet effect observed experimentally. The implemented model fail to capture the inlet effect, but this is a well known and documented problem in constitutive rheological models coupled with CFD.

The implemented model shows qualitatively the expected results wrt. normal and shear stresses when tested in benchmark geometries, but is plagued with convergence issues at high Deborah numbers, something that is also well documented in literature for these models.

Simulations on the inlet geometry used experimentally was conducted to study the proportionality between maximum inlet stretch rate and wall shear rate. The result indicates that even though close to constant and approaching a constant value with flow rate the ratio of stretch to wall shear rate appear to be Reynolds number dependent.

From the simulations it is shown that the proportionality between wall shear rate and maximum stretch rate is ~0.15-0.25 for Newtonian fluids in the experimental geometry. The validity of using this ratio due to the possibility of a different flow field with stretch thickening non Newtonian polymer solutions are not certain. This ratio can still give a give a semi-quantitative measure of the maximum stretch rate the polymer is submitted to, and thus provide a valuable starting point for more studies on extensional thickening and degradation studies in parallel with CFD simulations.

The validity of using a single “maximum” stretch rate to explain the inlet phenomena is not certain, as in complex flows the fluid will be submitted to a range of stretch rates that are transient in the fluid reference frame.

8 Further work

Further work on short capillary pipes of different lengths may provide more insight into the mechanisms behind both mechanical degradation and the “stretch thickening” effect causing increased apparent viscosity. This work has only considered one polymer and two concentrations, and further work on different molecular weight polymers, concentrations and ion concentrations should be conducted to provide more data for comparison with behaviour in porous media.

Even though this work shows that the increase in apparent viscosity is a inlet effect, the exact mechanisms behind this inlet effect are not fully understood. Further work using transparent geometries and image based particle velocimetry (or some other similar technique) might help increase understanding of the inlet effect, as well as controlling the validity of using a stretch/shear ratio for interpretation that are based on Newtonian fluids.

Due to time limitations the mechanical degradation effects was only partly studied in this work. Further work on capillary tubes of different lengths, together with different rheological measurements of the effluent shows promise in understanding degradation mechanisms, and what strains that primarily cause degradation. Gel permeation chromatography (GPC) and traditional rheological measurements of “fresh” polymer solutions as well as effluent from easily defined geometries, such as different length capillaries will likely be a good approach.

Overall a lot more work on the flow behaviour of HPAAM and other viscoelastic fluids in general are needed to provide an understanding of the phenomena observed experimentally in both porous media and more simple geometries such as the capillary tubes in this work. In comparing literature there exists discrepancies in numerical simulations, experimental results and rheometric devices. Measurements methods of “extensional” viscosity are not yet fully developed, with order of magnitude differences in results from one apparatus to the other. Based on this it seems the best approach for further work on the extensional inlet effects and mechanical degradation is one compromising of a range of methods in parallel with CFD simulations.

References

[1] D. W. Green, "Enhanced oil recovery," G. P. Willhite, Ed., ed. Richardson, TX: Henry L. Doherty Memorial Fund of AIME, Society of Petroleum Engineers, 1998, p. book.

[2] A. Thomas, N. Gaillard, and C. Favero, "Some Key Features to Consider When Studying Acrylamide-Based Polymers for Chemical Enhanced Oil Recovery," *Oil Gas Sci. Technol. – Rev. IFP Energies nouvelles,* vol. 67, pp. 887-902, 2012.

[3] A. Stavland, H. Jonsbraten, A. Lohne, A. Moen, and N. H. Giske, "Polymer Flooding - Flow Properties in Porous Media versus Rheological Parameters," 2010.

[4] R. B. Bird, *Dynamics of polymeric liquids*. New York: Wiley, 1987.

[5] J. M. Gasiorek, J. F. Douglas, J. A. Swaffield, and L. B. Jack, *Fluid mechanics*. Harlow: Pearson/Prentice Hall, 2005.

[6] A. Stavland, H. Moradi, and D. G. Hatzignatiou, "Experimental Investigation of Polymer Flow through Water- and Oil-Wet Berea Sandstone Core Samples," 2013.

[7] C. J. S. Petrie, "Extensional viscosity: A critical discussion," *Journal of Non-Newtonian Fluid Mechanics,* vol. 137, pp. 15-23, 8/30/ 2006.

[8] D.F. James and K. Walters, "A critical appraisal of available methods for the measurement of extensional properties of mobile systems," in *Techniques of Rheological Measurement*, ed New York: Elsevier, 1994.

[9] Yongpeng Sun, Laila Saleh, and B. Bai, "Ch.8 Measurement and Impact Factors of Polymer Rheology in Porous Media," in *Rheology*, J. D. Vincente, Ed., ed: InTech, 2012.

[10] G. Chauveteau, "Molecular Interpretation of Several Different Properties of Flow of Coiled Polymer Solutions Through Porous Media in Oil Recovery Conditions," 1981.

[11] K. S. Sorbie and L. J. Roberts, "A Model for Calculating Polymer Injectivity Including the Effects of Shear Degradation," 1984.

[12] J. G. Southwick and C. W. Manke, "Molecular Degradation, Injectivity, and Elastic Properties of Polymer Solutions," 1988/11/1/ 1988.

[13] R. S. Seright, J. M. Seheult, and T. Talashek, "Injectivity Characteristics of EOR Polymers," 2009.

[14] G. H. McKinley , S. L. Anna, A. Tripathi, and M. Yao, "Extensional rheometry of polymeric fluids and the uniaxial elongation of viscoelastic filaments," presented at the Annual Meeting of The International Polymer Processing Society, 1999.

[15] A. Kreiba, "The Rheological Properties of Aqueous Polyacrylamide Solutions," MSc Thesis, Mechanical Engineering, Concordia University, Montral, Quebec, Canada, 2000.

[16] A. Bhardwaj, E. Miller, and J. P. Rothstein, "Filament stretching and capillary breakup extensional rheometry measurements of viscoelastic wormlike micelle solutions," *Journal of Rheology (1978-present),* vol. 51, pp. 693-719, 2007.

[17] A. Lanzaro, "Microscopic flows of aqueous polyacrylamide solutions: a quantitative study," PhD Thesis, Faculty of Engineering and Physical Sciences, University of Manchester, Manchester England, 2011.

[18] R. G. Owens and T. N. Phillips, *Computational rheology*. London: Imperial College Press, 2002.

[19] P. J. Oliveira, "Method for time-dependent simulations of viscoelastic flows: vortex shedding behind cylinder," *Journal of Non-Newtonian Fluid Mechanics,* vol. 101, pp. 113-137, // 2001.

[20] G. N. Rocha, R. J. Poole, M. A. Alves, and P. J. Oliveira, "On extensibility effects in the cross-slot flow bifurcation," *Journal of Non-Newtonian Fluid Mechanics,* vol. 156, pp. 58-69, 1// 2009.

[21] A. M. Afonso, P. J. Oliviera, F. T. Pinho, and M. A. Alves, "Dynamics of high-Deborah-number entry flows: a numerical study," *Journal of Fluid Mechanics,* vol. 677, pp. 272-304, 2011.

[22] H. R. Tamaddon-Jahromi, M. F. Webster, and K. Walters, "Predicting numerically the large increases in extra pressure drop when boger fluids flow through axisymmetric contractions," *Natural Science,* vol. 2, 2010.

[23] A. Afsharpoor, M. T. Balhoff, R. Bonnecaze, and C. Huh, "CFD modeling of the effect of polymer elasticity on residual oil saturation at the pore-scale," *Journal of Petroleum Science and Engineering,* vol. 94–95, pp. 79-88, 9// 2012.

[24] H. K. Versteeg and W. Malalasekera, *An introduction to computational fluid dynamics: the finite volume method*. Harlow: Pearson/Prentice Hall, 2007.

[25] ANSYS-Inc, *Ansys Fluent Users's Guide*, 14 ed. vol. 14, 2011.

[26] ANSYS-Inc, "ANSYS Fluent UDF Manual," vol. 14, ed, 2011.

[27] ANSYS-Inc, *Ansys Fluent Theory Guide*, 14 ed. vol. 14, 2011.

Appendix A Experimental Data

Pipe length [m]	0,35	Fill rate 10ml/min	
Pipe ID [µm]	1310	L/R	534,351145
	Pressure loss [bar]	Flow Rate [ml/min]	
Water	0,08000	100	
	0,03750	45	
	0,03320	40	
	0,02840	35	
	0,02409	30	
	0,02007	25	
	0,01567	20	
	0,01155	15	
	0,00774	10	
	0,00382	5	
	0,00323	4	
	0,00245	3	
	0,00157	2	
	0,00078	1	
	0,00039	0,5	
	Pressure loss [bar]	Flow Rate [ml/min]	
FP3630s 600ppm	0,24000	100	
	0,03280	15	
	0,02223	10	
	0,01097	5	
	0,00901	4	
	0,00695	3	
	0,00490	2	
	0,00264	1	
	0,00127	0,5	
	0,00098	0,4	
	0,00078	0,3	
	0,00054	0,2	
	0,00029	0,1	
	Pressure loss [bar]	Flow Rate [ml/min]	
FP3630s 1500ppm	0,60000	100	
	0,18100	50	
	0,04162	10	
	0,02203	5	
	0,01831	4	
	0,01449	3	
	0,01087	2	
	0,00617	1	
	0,00343	0,5	
	0,00304	0,4	
	0,00235	0,3	
	0,00176	0,2	
	0,00127	0,1	

Pipe length [m]	0,033	Fill rate 10ml/min
Pipe ID [µm]	307	L/R
	Pressure loss [bar]	Flow Rate [ml/min]
Water	0,025	1
	0,052	2
	0,089	3
	0,126	4
	0,17	5
	0,217	6
	0,27	7
	0,326	8
	0,385	9
	0,443	10
	0,51	11
	0,57	12
	0,64	13
	0,71	14
	0,77	15
	0,83	16
	0,96	18
	1,08	20
	1,46	25
	Pressure loss [bar]	Flow Rate [ml/min]
FP3630s 600ppm	0,036	0,2
	0,11	0,4
	0,17	0,6
	0,234	0,8
	0,286	1
	0,42	1,5
	0,53	2
	0,63	2,5
	0,71	3
	0,88	4,5
	0,97	5
	1,165	6
	1,655	7
	1,92	8
	2,17	9
	2,38	10
	3,71	12
	4,15	14
	4,88	16
	5,37	18
	5,6	20

214,983713

FP3630s 1500ppm	Pressure loss [bar]	Flow Rate [ml/min]
	0,038	0,2
	0,085	0,4
	0,145	0,6
	0,215	0,8
	0,28	1
	0,45	1,5
	0,58	2
	0,7	2,5
	0,78	3
	0,98	4,5
	1,14	5
	1,37	6
	1,6	7
	1,72	8
	1,94	9
	2,15	10
	2,55	12
	3	14
	3,3	16
	3,8	18
	4,4	20

Pipe length [m]	0,0755	Fill rate 10ml/min	
Pipe ID [µm]	325	L/R	464,615385
	Pressure loss [bar]	Flow Rate [ml/min]	
Water	0,023	0,5	
	0,046	1	
	0,095	2	
	0,145	3	
	0,195	4	
	0,245	5	
	0,3	6	
	0,356	7	
	0,415	8	
	0,47	9	
	0,53	10	
	0,59	11	
	0,655	12	
	0,72	13	
	0,78	14	
	0,85	15	
	0,92	16	
	1,06	18	
	1,21	20	
	1,61	25	
FP3630s 600ppm	Pressure loss [bar]	Flow Rate [ml/min]	
	0,015	0,1	
	0,02	0,15	
	0,028	0,2	
	0,083	0,4	
	0,111	0,6	
	0,183	0,8	
	0,235	1	
	0,46	2	
	0,68	3	
	0,92	4	
	1,05	5	
	1,27	6	
	1,45	7	
	1,66	8	
	1,86	9	
	2,05	10	
	2,39	12	
	2,78	14	
	3,18	16	
	3,55	18	
	3,97	20	
	5	25	

FP3630s 1500ppm	Pressure loss [bar]	Flow Rate [ml/min]
	0,03	0,1
	0,041	0,15
	0,065	0,2
	0,129	0,4
	0,205	0,6
	0,28	0,8
	0,355	1
	0,73	2
	0,75	3
	1,08	4
	1,35	5
	1,65	6
	2	7
	2,35	8
	2,65	9
	3	10
	3,55	12
	4,25	14
	4,7	16
	5,3	18
	5,85	20

Pipe length [m]	1,89	Fill rate 10ml/min
Pipe ID [µm]	325	L/R
	Pressure loss [bar]	Flow Rate [ml/min]
Water	0,23	0,2
	0,46	0,4
	0,7	0,6
	0,93	0,8
	1,17	1
	2,32	2
	3,48	3
	4,62	4
	5,79	5
	6,97	6
	8,1	7
	9,2	8
	10,4	9
	11,7	10
	14,3	12
	17,1	14
	20	16
FP3630s 600ppm	Pressure loss [bar]	Flow Rate [ml/min]
	0,33	0,1
	0,66	0,2
	1,335	0,4
	1,94	0,6
	2,52	0,8
	3,05	1
	5,76	2
	10,7	4
	15,6	6
	20,5	8
	25,5	10
	30,5	12
	35,5	14
	40,6	16
	45,8	18
	50,9	20
FP3630s 1500ppm	Pressure loss [bar]	Flow Rate [ml/min]
	0,38	0,05
	0,7	0,1
	1,29	0,2
	2,37	0,4
	3,39	0,6
	4,28	0,8
	5,12	1
	8,8	2
	15,7	4
	22,3	6
	29,1	8
	35,7	10
	42,1	12
	48,4	14
	54,6	16
	60,9	18
	67,2	20

11631

Appendix B Oldroyd B Fluent model

```
#include "udf.h"

/*******************/
/*Defining constants*/
/*******************/


#define MU_S 0.001   /*Solvent viscosity*/
#define VISC_P 0.001 /*Polymer viscosity*/
#define RHO 998.00   /*Density*/
#define KAPPAV 0.05  /*Time constant*/

/*************************************************************************************
*********/
/*User defined scalars to store the stress tensor T_ij*/
/*************************************************************************************
********/

enum
{
       T11,
       T12,
       T21,
       T22,
       N_REQUIRED_UDS
};

/*********************************/
/*Defining FLUENT fluid properties*/
/*********************************/

DEFINE_PROPERTY(density, c, t)
{
       return RHO;
}

DEFINE_PROPERTY(viscosity, c, t)
{
       return MU_S;
}

/*********************************************************/
/*Defining stress tensor and momentum source terms*
/*********************************************************/

DEFINE_SOURCE(T11_source, c, t, dS, eqn)
{


       dS[eqn] = RHO*(-1. / KAPPAV + 2 * C_U_RG(c, t)[0]);
       return  RHO*(2.*C_UDSI(c, t, T11)*C_U_RG(c, t)[0] + C_UDSI(c, t, T12)*C_U_RG(c,
t)[1] + C_UDSI(c, t, T21)*C_U_RG(c, t)[1]
              /*Upper convected derivative*/
             + (2 * VISC_P / KAPPAV)*C_U_RG(c, t)[0] - (C_UDSI(c, t, T11) / KAPPAV));

             /*Source*/

}

DEFINE_SOURCE(T12_source, c, t, dS, eqn)
```

```
{

       dS[eqn] = RHO*(-1. / KAPPAV + C_V_RG(c, t)[1] + C_U_RG(c, t)[0]);
       return RHO*(C_UDSI(c, t, T11)*C_V_RG(c, t)[0] + C_UDSI(c, t, T12)*C_V_RG(c,
t)[1] +
              C_UDSI(c, t, T12)*C_U_RG(c, t)[0] + C_UDSI(c, t, T22)*C_U_RG(c, t)[1]

              /*Upper convected derivative*/
              + (2 * VISC_P / KAPPAV)*0.5*(C_V_RG(c, t)[0] + C_U_RG(c, t)[1]) -
(C_UDSI(c, t, T12) / KAPPAV));
              /*Source*/

}

DEFINE_SOURCE(T21_source, c, t, dS, eqn)
{

       dS[eqn] = RHO*(-1. / KAPPAV + C_U_RG(c, t)[0] + C_V_RG(c, t)[1]);
       return RHO*(C_UDSI(c, t, T21)*C_U_RG(c, t)[0] + C_UDSI(c, t, T22)*C_U_RG(c,
t)[1] +
              C_UDSI(c, t, T11)*C_V_RG(c, t)[0] + C_UDSI(c, t, T21)*C_V_RG(c, t)[1]

                     /*Upper convected derivative*/
              + (2 * VISC_P / KAPPAV)*0.5*(C_V_RG(c, t)[0] + C_U_RG(c, t)[1]) -
(C_UDSI(c, t, T21) / KAPPAV));
                     /*Source*/

}
DEFINE_SOURCE(T22_source, c, t, dS, eqn)
{

       dS[eqn] = RHO*(-1. / KAPPAV + 2 * C_V_RG(c, t)[1]);
       return  RHO*(2.*C_UDSI(c, t, T22)*C_V_RG(c, t)[1] + C_UDSI(c, t, T12)*C_V_RG(c,
t)[0] + C_UDSI(c, t, T21)*C_V_RG(c, t)[0]
       /*Upper convected derivative*/
              + (2 * VISC_P / KAPPAV)*C_V_RG(c, t)[1] - (C_UDSI(c, t, T22) / KAPPAV));

                                                  /*Source*/

}
DEFINE_SOURCE(xmom_source, c, t, dS, eqn)
{
       dS[eqn] = 0.;
       return (C_UDSI_G(c, t, T11)[0] + C_UDSI_G(c, t, T12)[1]);
}
DEFINE_SOURCE(ymom_source, c, t, dS, eqn)
{

       dS[eqn] = 0.;
       return (C_UDSI_G(c, t, T21)[0]+C_UDSI_G(c, t, T22)[1]);

}
```

Appendix C Task description

FMH606 Master's Thesis

Title: Polymer flow in porous media

TUC supervisor: Knut Vågsæther

External partner: Statoil ASA

Task description:

- Literature study of different methods for calculating fluid stresses in porous media for both Newtonian and non-Newtonian liquids, e.g. HPAM (partially hydrolyzed polyacrylamide) and non-Newtonian rheology of polymer/water solutions.
- CFD simulation of polymer/water solution flow in different geometries including non-newtonian rheological effects and the validity of isotropic viscosity models with emphasis on dilatant (shear thickening) behaviour of polymer solutions in porous media.
- CFD simulation of non-Newtonian polymer solutions with vicoelastic effects using user defined functions in FLUENT/Open FOAM.
- Experimental study of apparent viscosity for polymer solutions in shear and high normal stress flow conditions.
- Comparison of conventional methods of calculating fluid stresses in porous media (e.g. shear rate by capillary bundle method) with CFD simulations for Newtonian and non-Newtonian liquids.
- Study the link between fluid shear stress, normal stress and mechanical degradation in polymer solutions.

Task background:

Using polymers for well injection to enhance oil recovery has been used for many years but the behavior of the polymer in porous media with respect to apparent viscosity and mechanical degradation is not well understood.

Student category: Reserved for Christian Berg

Practical arrangements: The student will work at TUC.

Signatures:

Student (date and signature):

Supervisor (date and signature):